GEORGE C. MARSHALL SPACE FLIGHT CENTER

HUNTSVILLE, ALABAMA

AERODYNAMIC ANALYSIS OF TEKTITES AND THEIR PARENT BODIES

by

E. W. Adams and R. M. Huffaker

National Aeronautics and Space Administration

NASA

AERODYNAMIC ANALYSIS OF TEKTITES AND THEIR PARENT BODIES

by

E. W. Adams and R. M. Huffaker

to be presented at the

Third International Space Science Symposium

Washington, D. C.

May 1 - 8, 1962

LIST OF FIGURES

LIST OF FIGURES (CONT'D)

LIST OF SYMBOLS

$A = \pi R^2(0)$	cm^2	Area of maximum cross section in fig. 4
a	m/sec^2	Deceleration
α	1/m	Absorption coefficient for thermal radiation
c_D		Drag coefficient
c_p	kcal/kg °K	Specific heat at constant pressure
D	km	horizontal range covered in flight
$g = 9.81$	m/sec^2	Gravity constant at sea level altitude
H	km	Flight altitude
h	kg/m^2sec	Heat transfer coefficient
h_e	kcal/kg	Enthalpy of air at outer edge of boundary layer
h_s	kcal/kg	Enthalpy of air at surface
h_v	kcal/kg	Heat of evaporation
k	kcal/m °K sec	Thermal conductivity
M		Flight Mach number
m	kg_m	Mass
p_e	kg/m^2	Air pressure at outer edge of boundary layer
p_{v_1}	kg/m^2	Vapor pressure of tektite material
p_{v_2}	kg/m^2	Vapor pressure of quartz
q_{aero}	$kcal/m^2sec$	Aerodynamic heat transfer to evaporating surface
$\bar{q}_{aero}$	$kcal/m^2sec$	Aerodynamic heat transfer to non-evaporating surface
q_{bl}	$kcal/m^2sec$	Heat blocked by evaporation and vapor diffusion
q_{rad}	$kcal/m^2sec$	Heat radiated from surface into air

LIST OF SYMBOLS (CONT'D)

R and R*	m	Defined in fig. 4
t	sec	Time
T	°K	Temperature
u	mm/sec	Velocity component of melt flow parallel to surface
v	mm/sec	Velocity component of melt flow normal to surface
v_∞	mm/sec	Ablation speed at stagnation point
v_s	mm/sec	Evaporation speed of melt at stagnation point
V	km/sec	Flight speed
W	gram	Weight
x	m	Coordinate parallel to surface, fig. 4
y or z	m	Coordinate normal to surface, fig. 4
γ	kg/m^3	Specific weight
ϵ		Emissivity constant
θ		Angle of flight trajectory relative to earth's horizon
μ	$kg/sec/m^2$	Viscosity

Subscripts

f	final, i.e., impact time at sea level altitude
i	initial, i.e., entry time at outer edge of earth's atmosphere
max	maximum value
s	surface at stagnation point

SUMMARY

Tektites are small glassy bodies which are found in well-defined areas and, in general, belong to one of a few well-defined classes of geometrical shapes. The largest strewn field covers most of southeast Asia, another field most of Australia. Tektites are unrelated to the geological formations in which they are found; therefore, they must have been hurled up somewhere by violent natural events and carried in flight into the strewn fields. This brings up the problem of the terrestrial or extraterrestrial origin of the tektites. Aerodynamic analysis is employed to investigate tektite flight in the atmosphere of the earth and thus to impose pertinent restrictions on the large number of possible hypotheses about tektite origin. In an experimental study at the Ames Research Center of NASA, it has been shown that glass spheres, when exposed to heating rates as would be experienced in hypersonic flight, become strikingly similar to the shapes of the button-type australites. Ablation and trajectory analysis indicate that an average-weight button-type australite entered the atmosphere at shallow angles relative to earth's horizon and with entry speeds in excess of 6.5 km/sec in order to experience the observed average figure of more than 70% mass loss in flight as compared to the volume of the sphere from which the button was derived.

The following additional results of trajectory and ablation analysis are presented pertaining to the origin of these glass spheres:

(1) The glass spheres could originate from the earth's surface only in the extremely unlikely case that a highly transparent glassy body of considerably more than 10,000 tons weight departs with more than 10 km/sec from the earth and releases liquid drops from its ablating surface.

(2) The glass spheres could be released as liquid drops from a glassy parent meteor which is sufficiently transparent to thermal radiation.

(3) Fusion of siliceous rock into glass by aerodynamic effects is impossible.

Tektites are shown to be remnants of extraterrestrial glassy bodies which entered the earth's atmosphere in skipping flight and, probably, were removed by meteor impact from the moon. Glassy meteors which descend directly or stony meteors cannot release meteorites of well-defined shapes like tektites.

I. INTRODUCTION

Tektites are small glassy bodies which are found in well defined areas. The largest so-called strewn field covers most of Southeast Asia, and another strewn field covers most of Australia; smaller fields are located in Texas, Georgia, Ghana, Bohemia, and Moravia. All tektites have a family-like chemical composition and are unrelated to the geological formations in which they are found; therefore, they must have been hurled up somewhere by violent natural events and carried in flight into the strewn fields. Available evidence, e.g., radioactive dating, proposes, according to p. 118 of ref. 5, "that the different groups of tektites from the several zones of occurrence are separated in their time of arrival by considerable periods of time and that there must thus have been more than one shower of tektites during the earth's geological history." The material thrown up was either already glassy, due to meteor impact or volcanic action, or was fused into glass by aerodynamic heating in flight. In addition to such aerothermodynamic effects during a hypothetical first flight phase in an atmosphere, all the australites and some javaites show a superficial second melting period resulting in a few peculiar types of surface sculpturings and well defined shapes, which can be explained by ablation during hypersonic flight in the earth's atmosphere, as will be shown in this paper.

It has not yet been possible to prove by chemical or physical analysis of natural tekites whether tektite-flight started at the earth's surface or at some extraterrestrial point of departure. The glassy uncrystallized substance includes 68% - 80% silica, 9% - 16% Al_2O_3, etc. The complete absence of crystals and a slightly different chemical composition distinguishes tektite glass from glassy ejacta, e.g., consisting of solidified ash from volcanic eruptions or from steam locomotives. According to ref. 7, very small quantities of nickel-iron spherules have been found among the minor constituents of some tektites. Since meteors are the only natural source of nickel-iron, meteor impact must then have caused the flight of tektites or of their parent bodies which released tektites in flight. Since Al^{26} with a half-life of 10^6 years is generated by prolonged exposure to cosmic radiation, its absence in 79 tektites taken from the Far East and Australia, according to ref. 22, yields the conclusions "(1) if tektites arrived as small unshielded bodies, their 'flight' or cosmic-ray exposure time was less than 10,000 years; (2) if they arrived in a large, well-shielded body, this 'prototektite' body must have had a radius $\geq$ 95 m."

For a tektite cluster in arbitrary orbit in the solar system, the life expectation before an encounter with the earth is very much larger than 10,000 years, according to ref. 18. In addition, stability reasoning in ref. 21 establishes a minimum density of 10^{-6} grams/cm^3 for such a cluster, which, in case of its encounter with the earth, would pile up tektite layers of 100 grams/cm^2 over southern Australia. Therefore,

tektite clusters of extraterrestrial origin arriving at the earth most likely originate from the moon and their entry speed into the earth's atmosphere is limited by approximately the escape speed, 11.2 km/sec, of the earth-moon system.

These general statements are compatible with a large number of possible hypotheses about the origin of the tektites. Whereas the possibility of ablative shaping of tektites in flight has been discussed before in references 11, 13, 14, and 19, only the recent experimental and theoretical advances in the field of missile and space vehicle re-entry furnish the calculation methods needed to analyze tektite flight in the earth's atmosphere and thus to impose further restrictions on the variety of hypotheses. The available calculation methods for trajectory and ablation analysis are applicable if the object is a simple-shaped body of revolution, consisting of a known material, and flying at zero angle of attack. With the exception of some uncertainty about material properties, these conditions are fulfilled for the button-type australites, whose final shape appears in figures 1 and 2. The results to be discussed rest on the well-known trajectory equations for bodies of variable mass and on a calculation method for ablating glass or stone bodies. This method is described in ref. 2 and in unpublished reports by the same author. Comparison of ablation thicknesses calculated by use of this method to experimental ablation data for a glassy material shows less than 10% deviation.

Experimental results and aerothermodynamic analysis are employed in sections 2 - 4 to determine the initial shape and the possible entry conditions of the button-type australites at the beginning of their final descent. Possible previous flight phases in the earth's atmosphere are then studied in section V to investigate (1) whether tektite-flight could have started at the earth's surface or at the outer edge of the atmosphere only, (2) whether tektites could have been released in flight from a parent meteor, and (3) whether the fusion of siliceous rock into glass is possible by aerodynamic heating in the atmosphere.

The authors are indebted for very helpful discussions to Dr. John A. O'Keefe of the Goddard Space Flight Center, Greenbelt, Maryland and to Mr. Werner K. Dahm, Marshall Space Flight Center, Huntsville, Alabama.

II. EXPERIMENTAL EVIDENCE FOR THE SHAPING OF THE BUTTON-TYPE AUSTRALITES BY AERODYNAMIC ABLATION

Chapman, in ref. 9, presents conclusive experimental proof that glass spheres, when placed in an electric-arc jet tunnel and exposed to heating rates of the order of those experienced in hypersonic flight, become strikingly similar to button-type australites. This similarity comprises, firstly, a peculiar system of ring waves on the ablated front face, secondly, a coiled circumferential flange made of solidified melt,

and finally, opposite the stagnation point and enclosed by the flange, a spherical remainder of the original surface shape. This remainder is rough and pitted in case of the natural buttons as is seen in fig. 2. Fig. 3 shows a glass rod whose front face ablated in an electric-arc jet facility. The ring waves and the flange are clearly visible in fig. 3. The existence of a systematic deformation of the striae which is confined to a very thin layer underneath the surface of both the natural and the artificial buttons shows, according to ref. 9, that the ablation of the natural buttons was by aerodynamic heating of rigid glass and not by aerodynamic pressure acting on soft glass, since the latter would have distorted the striae pattern to a considerable depth below the surface. Chapman's experimental work confirms beyond doubt the hypothesis that the button-type australites were shaped by aerodynamic ablation from glass spheres, whose curvatures are identical to those of the pitted posterior surfaces of natural buttons.

III. THEORETICAL EVIDENCE FOR THE ABLATION OF AUSTRALITES IN DESCENDING FLIGHT

The inspection of surface sculpturings on discovered australites reveals, according to pp. 74 - 76 of ref. 5, that they were derived from bodies of revolution and, in the majority of cases, from spheres. Chapman points out on pp. 16 - 19 of ref. 9 that an oscillation about any axis other than the flight axis, whether initially present or induced by disturbances in flight, is rapidly damped by the continuously increasing magnitude of the surface pressure distribution in descending flight, whereas this damping effect would be absent in ascending flight. The decrease in curvature at the point where melting begins on a sphere causes a rearward departure of the aerodynamic center (of the pressure distribution) from the center of gravity. The corresponding unbalanced moment about the center of gravity tends to align the stagnation point of the body of revolution, the center of gravity, and the aerodynamic center, so that this will be the stable flight attitude.

For a glass sphere of 1.3 cm radius in ascending flight with an initial speed of 8 km/sec at sea level altitude, a simple calculation yields an initial deceleration of 96,000 g and, therefore, together with Chapman's stability reasoning, rules out the departure from the earth's surface of a cluster of tektites.

These considerations still leave the possibility of liquid droplets released from the melting surface of a large solid rock having been hurled up from the earth's surface by meteor impact. The material evidently must be sufficiently rigid in order to avoid immediate disintegration. The initial speed must be sufficiently high and the initial trajectory angle sufficiently shallow if an area of the size of Australia is to be covered by fragments of this rock or a cluster of big rocks hurled up by the same event. As an example, a hemisphere with initial

radius R(0) = 6.74 m, consisting of siliceous rock and weighing 1700 tons, is being considered in flight attitude according to fig. 4. The initial speed at sea level altitude is assumed to be 10 km/sec and the angle of departure 15° relative to the earth's horizon. The initial deceleration ≅ 500 g. After 1.8 sec flight time, the hemisphere has gained the altitude H = 3.39 km, and the speed is 5.64 km/sec. The stagnation point values of the aerodynamic heat transfer rate $\bar{q}_{aero}$ and of the surface temperature T_s are at that time 2652 kcal/m^2 sec and 3003 °K, respectively. The surface temperature gradient in a direction normal to the surface has then a value of 1.8 x 10^6 °K/m and the temperature drops by 2084 °K in a layer of only 1.76 mm thickness. The surface recedes 1.4 mm during the first 1.8 sec flight time, 51% of which is due to melt flow. If gas radiation is considered in addition to convective heating, the surface would boil rapidly and the heated layer would become thinner, so that the body being considered cannot release liquid droplets if it consists of opaque stone.

If the material were glassy and transparent to thermal radiation, the thickness of the heated layer would considerably increase, as is brought out by the discussions in section V. After 20 sec flight time, the velocity is only 2.093 km/sec, the altitude only 16.3 km, and the surface temperature at the stagnation point only 1291 °K for the body being considered. It is seen that liquid droplets released from the ablating surface of this body, if it is transparent, cannot leave the atmosphere and then re-enter at speeds between 6 and 11.2 km/sec, as is required by the results of trajectory and ablation analysis in section IV. Terrestrial origin of tektites then is restricted to the extremely unlikely case of a highly transparent glassy body with $\gg$ 1700 tons departing from the earth's surface $>$ 6 km/sec.

IV. TRAJECTORY AND ABLATION ANALYSIS FOR THE FINAL DESCENT OF THE BUTTON-TYPE AUSTRALITES

By employing the steady-state approximation derived in ref. 6 for the ablation process, Chapman (ref. 8) was the first to analyze the descent of button-type australites under the assumption of small or moderate ablative mass losses so that the variable mass could be approximated in the trajectory calculations by the average of the masses at the beginning and at the end of the flight. Ref. 4 presents a summary of a renewed study, to be discussed extensively in this section, of the final descent of button-type australites by employing combined non-stationary trajectory and ablation analysis in order to obtain results for the melting and evaporation history up to 100% ablation. The large deviations of quasi-steady ablation analysis from exact non-stationary analysis are exemplified by the results presented in ref. 3.

If an axially symmetric body of revolution flies at zero angle of attack, the conduction of heat and the ablation can be treated along the

body axis $0\text{-}S_o$ in fig. 4 without reference to the neighboring cross sections because of the extremum characteristics of the solution along the axis $0\text{-}S_o$. The front face ablation of the glass spheres from which the button-type australites were derived and the formation of a flange can be approximated by a simplified model that is hemispheric at the entry altitude H = 150 km above sea level. In order to check the dependence of the results on the geometric model employed, an initially spherical model was also investigated whose front half is supposed to ablate as shown in fig. 4. A comparison of results for the two models indicates very little difference, (See table 1). The calculated results prove that the flow of air is laminar on the entire surface of the assumed hemispheric model during the ablation period. Other studies (e.g., ref. 2) show that the total ablation decreases under this condition as the distance from the stagnation point increases. The ablation process, which is calculated only along $0\text{-}S_o$, is supposed to convert the hemispheric shape $A\text{-}S_o\text{-}B\text{-}0\text{-}A$ in fig. 4 into the section A-S(t)-B-0-A of a sphere completely defined by the thickness R*(t) of the model. The weights of the glass spheres from which the button-type australites were derived by ablation vary in the limits 5 - 20 grams, according to p. 80 of ref. 5. This yields the limiting initial radii R(0) = 0.99 cm and R(0) = 1.58 cm of the hemispheric model. Results have been calculated for the radii R(0) = 0.65 cm and R(0) = 1.30 cm, which correspond to initial weights 1.38 and 11.04 grams, respectively. A constant drag coefficient of $c_D = 2.5$ was assumed for the trajectory calculations in the free-molecular region of the air; c_D was calculated as a function of R*(t)/R(0) and of the flight Mach number, M(t), in the continuum flow region of the air. The trajectory and ablation analysis was carried out on an IBM 7090 computer by use of time steps between 10^{-3} and 10^{-1} sec. The following material properties of the supposedly opaque material were employed in the calculations: thermal conductivity $k = 5 \times 10^{-4}$ kcal/m °K sec according to p. 162 of ref. 5; specific heat $c_p = 0.21$ kcal/kg °K according to ref. 12; surface emissivity constant $\epsilon = 0.4$ (estimated); and viscosity function $\mu(T) = 0.0102 \exp [(44{,}891/T\ °K) - 14.541]$ kg sec/m^2 according to ref. 23. Since measurements of the vapor pressure $p_v(T)$ of tektite material have not yet been published, the actually employed function, namely, $p_{v1}(T) = 13.595\exp[30.01-(57{,}250/T\ °K)]$ kg/m^2, was obtained from the vapor pressure of fused silica, $p_{v2}(T) = 15{,}498 \exp [18.41 - (58{,}176/T\ °K)]$ kg/m^2, ref. 20, by lowering the boiling point at one atmosphere from 3070 °K to 2500 °K to account for the volatile component in tektites, whose silica content is only 68% - 80%.

For the initially hemispheric model of button-type australites shown in fig. 4 with the material properties listed in the preceding paragraph, the figures 5 through 15 present curves of constant performance parameters as functions of entry speed V_i km/sec and entry angle θ_i at entry altitude H = 150 km above sea level. The material properties were changed in a few typical cases to take the following values: firstly, $k = 4 \times 10^{-4}$ kcal/m °K sec and $c_p = 0.29$ kcal/kg °K; secondly, $\epsilon = 0.05$. The resulting

changes in the relative mass loss, $[1 - m(t_f)/m(0)]$, are smaller than 6% as compared to the results presented in fig. 5. The comparison of the solid lines in figures 5 and 6 shows, however, that the uncertainty about the vapor pressure of tektite material has considerable effect on the results.

The curves for R(0) = 1.3 cm (initial weight of 11.04 grams) in figures 5 and 6 are typical for the discovered button-type australites since the spheres defined by the radii of the posterior surfaces of natural buttons have an average weight of 11 grams, according to p. 79 of ref. 5. The range of possible entry conditions can then be limited as follows in figures 5 and 6: (1) by the overshoot line since the final descent is considered, (2) according to p. 79 of ref. 5, by the ablation range of 70% - 90% for natural buttons with an initial weight of 11 grams, and (3) by the earth's escape speed, 11.2 km/sec. The last condition is valid for both a cluster of tektites entering the earth's atmosphere for the first time, according to evidence in section I pertaining to the lunar origin of such a cluster, and also for re-entering solidified droplets which were released from an ablating parent body in a manner to be described in section V. The possible entry conditions are then $7 \leq V_i \leq 11.2$ km/sec and $0 \leq \theta_i \leq 6°$ in case of the function $p_{v1}(T)$ and $6.5 \leq V_i \leq 11.2$ km/sec and $0 \leq \theta_i \leq 29°$ in case of the function $p_{v2}(T)$.

Table 2, which follows from evaluating figures 5 through 15, explains the dependence of the results on the relevant parameters V_i, θ_i, m(0), and $p_v(T)$. This dependence is predominantly determined by the aerodynamic heating pulse and by the shielding mass transfer effect. A smaller percentage of the kinetic energy converted into heat reaches the surface as the heat pulse is shifted to lower altitudes, where a higher portion of the generated heat remains in the denser air. The case is clearest for the change of θ_i since this causes no change in the kinetic energy and only a relatively small increase in the mass transfer effect according to table 2.

Any rise of the enthalpy difference $(h_e - h_s)$ across the air boundary layer causes an increase of the surface temperature T_s and, correspondingly, of the flow rate and evaporation rate of melt and of the emission of radiation from the surface. The vaporization process absorbs heat; also, the heat transfer coefficient, h, decreases due to the diffusion of vapor across the air boundary layer. The aerodynamic heat transfer rate at the wall, $q_{aero}(t) = h(h_e - h_s)$ kcal/m^2 sec, therefore, increases at a smaller rate than the enthalpy difference $(h_e - h_s)$. Since there is only convective heating and negligible gas radiation for the small bodies under discussion, the surface temperature may tend toward the boiling point but it cannot reach this point. If the intensity of the heat pulse increases at a constant altitude, as in case of a rise of V_i, small increases of the surface temperature are sufficient to raise both the evaporation rate and the shielding mass transfer effect at such a steep rate as to cope with

any increase of $(h_e - h_s)$. If the heat pulse is shifted to lower altitudes, the evaporation rate decreases unless the surface temperature considerably rises, as table 2 shows for an increase θ_i.

If the higher vapor pressure function $p_{v1}(T)$ is replaced by the lower function $p_{v2}(T)$, the necessary shielding mass transfer effect requires considerably higher surface temperatures and, therefore, is accompanied by higher melt flow rates (table 2). The comparison of the solid lines in figures 5 and 6 indicates a strong increase of the relative mass loss $[1 - m(t_f)/m(0)]$ when $p_{v2}(T)$ is substituted for $p_{v1}(T)$.

As an example for the 100 calculated solutions, figures 16 through 21 present one special solution which is defined by the entry speed V_i = 9 km/sec, the entry angle θ_i = 7° relative to the earth's horizon, the entry altitude H = 150 km above sea level, the vapor pressure function $p_{v1}(T)$, and the initial radius R(0) = 1.3 cm of the hemispheric model. The flight terminates at sea level altitude, H = 0 km, with the impact speed V_f = 17 m/sec and the nearly vertical impact angle θ_f = 89.99. The last calculated temperature profile along the axis of symmetry is nearly uniform with T = 780 °K at the altitude H = 11.54 km according to fig. 20; i.e., the body already has become rigid some time before impacting. It is seen that the aerodynamic heat pulse, $\bar{q}_{aero}(t)$, takes place at a slightly higher altitude than the deceleration pulse, a(t). The maximum deceleration has a value of 26 g. The ablation at the stagnation point, 43% of which is due to evaporation, starts in the free-molecular region of the air at 90 km altitude and ends in the hypersonic continuum flow region at flight Mach numbers > 4. The surface temperature closely follows the change of the aerodynamic heat transfer pulse, $\bar{q}_{aero}(t)$, to a non-evaporating surface.

For the initially hemispheric button model, whose performance as a function of time has been discussed in the preceding paragraph, fig. 20 presents temperature profiles T = T(z,t) °K along the body's z-axis as following from one-dimensional heat conduction analysis. The shaded portions adjacent to the instantaneous locations of the surface indicate the thickness of the melt flow. The deepest penetration of the molten layer is reached at time t = 100 sec when resolidification has just started. The corresponding calculated striae deformation due to previous melt flow in the solidified layer is shown in fig. 21a for the vicinity of the stagnation point. The straight line in fig. 21b shows the striae distortion as a function of the distance x from the stagnation point and the lines in fig. 21c feature the striae profiles underneath the surface for two distances x from the stagnation point. Fig. 22 shows the corresponding results for the striae deformation in case of an initially hemispheric model which enters with a speed of V_i = 6 km/sec and the angle θ_i = 2 and which suffers only 29% ablation in flight.

The following additional general conclusions can be drawn from the calculated cases: The impact at sea level altitude takes place in the range $88° \leq \theta_f \leq 90°$, i.e., in a nearly vertical direction. The impact speed is limited by $V_f \leq 28$ m/sec. The temperature level on the line 0-S(t) defined in fig. 4 is below 600 °K at impact time, so that plastic deformations due to the impact are impossible.

V. THE PARENT BODY HYPOTHESIS AND SKIPPING FLIGHT PHASES OF THE AUSTRALITES PRIOR TO THEIR FINAL DESCENT

a. Statement of the Problem

According to sections II and IV, observation, experiment, and analysis show that the button-type australites were rigid glass spheres which entered the earth's atmosphere at high altitude, shallow angles relative to the earth's horizon, and velocities in the range $6.5 \leq V_i \leq 11.2$ km/sec. Aerodynamic analysis in section III indicates that these initial conditions for the descent of the button-type australites are incompatible with a terrestrial origin of the flight.

Chapman assumes in ref. 8 that a cluster of glass spheres departs from the moon and traverses the earth's atmosphere, as is described in section IV. Since it is unlikely that glass spheres of radii $0.5 \leq R(0) \leq 1.35$ cm, as following from p. 79 of ref. 5, were hurled up from the moon by meteor impact, it is worthwhile to investigate whether the results of section IV are compatible with the arrival at the outer edge of the earth's atmosphere of stony or glassy meteors of any size and shape.

Hardcastle and Hanuš stipulated in references 13 and 14 that the surface of a stone meteor melts during hypersonic flight in the earth's atmosphere and sprays liquid droplets, which give rise to the characteristic forms of tektites as they cool. Since tektites consist of glassy material, the droplets must have possessed sufficiently high temperatures in order to fuse siliceous stone into glass. In general, aerodynamic heating is so great that the molten layer at the surface of a stony meteor is extremely thin, because of the low thermal diffusivity, the high viscosity of the melt, and its almost immediate evaporation. O'Keefe points out in ref. 15 that the evaporation rate of the melt might become sufficiently small if a grazing satellite orbit with small instantaneous heat transfer rates is considered, like the one of the Cyrillid shower. According to trajectory calculations published in ref. 16, only the liquid droplets released during the final stages in the earth's atmosphere of such a shallow orbit stay in the parent meteor's wake. Surface tension can be stipulated to convert the shapes of the liquid droplets flying in the skipping cluster into spheres according to detailed discussions in section Vc.

b. Arrival of a Stone Meteor

In order to simulate the Cyrillid flight, a hemispheric stone meteor of initial radius R(0) = 6.74 m, 1700 tons weight, and flight attitude according to fig. 4 is considered with speed V_i = 9 km/sec and trajectory angle $\theta_i = 2°$ at entry altitude H = 120 km. The initial temperature level is 300 °K; the surface temperature then is 425 °K at the stagnation point after 100 sec flight time, which corresponds to the minimum altitude of H = 103 km for this trajectory. The temperature amounts to 434 °K at this point after 200 sec flight time, which corresponds to the altitude H = 118 km, the flight speed V = 9.001 km/sec, and the trajectory angle $\theta_i = -2.2°$. The heat stored in the material is small since the temperature is 349 °K on the symmetry axis at a distance of only 1.59 cm beneath the surface.

Since the meteor stays in the free-molecular region of the air along this shallow trajectory with correspondingly small heat transfer rates, a steeper entry angle, $\theta_i = 6°$, and a higher entry speed, V_i = 11 km/sec, are now considered at the altitude H = 150 km. Under the assumption of negligible ablation, trajectory calculations yield a speed of V = 10.817 km/sec at the minimum altitude H = 47.91 km and the values V_f = 10.433 km/sec and $\theta_i = -6.85°$ for exit speed and exit angle at H = 150 km, respectively.

In addition to convective heating, the surface is subjected to radiative heating in the continuum flow and the slip flow regions of the air. The amount of radiation incident on the surface depends on the thickness of the radiating layer between shock front and surface and, therefore, is negligible for bodies as small as the button-type australites. The radiative heat transfer, however, becomes predominant for the big meteor under consideration.

The equilibrium gas radiation incident at the stagnation point is a function of altitude, speed, and body dimensions, and has been obtained from ref. 24 for the continuum flow region of the air and then extrapolated into the slip flow region. The radiation flux reaches a maximum value of 106,000 kcal/m^2 sec at the minimum altitude H = 47.91 km. At points other than the stagnation point, the gas radiation incident on the curved front surface of the hemispherical meteor was obtained from an approximative method which employs the distance between the shock front and the surface, as following from the theory of characteristics for a perfect gas, and the "equivalent gas volume" approach on p. 393 of ref. 10. The extremely high heat transfer rates cause the surface to boil, beginning shortly after entry into the slip flow region of the air. At the stagnation point, boiling starts at the altitude H = 106.8 km; at the distance x = 6 m from the stagnation point, measured around the curved front face, boiling starts at the altitude H = 106 km. The boiling process stops in ascending flight in the slip flow region and causes a removal of 98 cm along the symmetry

axis of the meteor. Due to the rapid recession of the boiling surface during a period of 232 sec, the thickness of the heated layer beneath the surface is smaller than 0.2 cm at the stagnation point. Since the omitted non-equilibrium radiation effects would only increase heat transfer and boiling rates, it may be concluded that a large stone meteor, consisting of opaque material, cannot release liquid droplets in skipping flight and thus cannot account for the origin of the button-type australites.

c. Arrival of a Glassy Meteor

If the parent meteor consists of a glassy substance of sufficiently low absorption coefficient per unit depth, α, the strong incident gas radiation heats a layer of appreciable thickness. In case of purely convective heat transfer, the surface evaporation process determines the temperature T_s of the boiling surface by the equation vapor pressure equals external pressure which is then approximately valid. In case of radiative heating, the boiling temperature of the surface is determined by the vacuum evaporation rate and by the absorption coefficient α; in general, T_s increases together with α. The temperature profile $T(z,t)$ across the radiatively heated layer depends on T_s and on α. If T_s is sufficiently high, vapor nuclei can be formed at non-homogeneous spots in the glass melt. Unless strong temperature gradients $\partial T/\partial z$ exist in the hot layer, there is no force available which drives the vapor bubbles towards the surface. The hot layer consists then of a spongy glass melt which offers little resistance to being removed from the body by the acting air forces. Since this mechanism rests on the existence of sufficiently high temperatures in the spongy layer, the separated liquid fragments possess low viscosity and break up readily in the air stream. This disintegration process of the fragments approaches its end when the fragments are sufficiently small so that surface tension can convert the spongy substance into relatively compact glassy drops. If these glassy drops leave the atmosphere in the wake of a skipping parent meteor, the air forces acting on the drops continuously decrease so that the drops tend to take spherical shape.

As a result of this disintegration process of the skipping parent meteor, a large number of small liquid drops fly in its wake. Since the individual drops experience more drag per unit mass than the large meteor, the majority of the liberated drops descend immediately according to O'Keefe's calculations in ref. 16, and only the drops liberated during the end of the parent meteor's ascending flight phase in the air stay in the wake. If the descending and the skipping clusters are sufficiently dense, the pressure fields acting on the individual members induce small velocity components normal to the flight direction. This effect and turbulence in the wake, as invoked by O'Keefe in ref. 16, explain why strewn fields of considerable length and width are covered by tektites.

The vapor bubbles in the spongy substance expand continuously in ascending flight because of the decrease of the external pressure. The bursting of the bubbles and the formation of drops by surface tension then yields a more compact substance in ascending flight than in descending flight. In both cases, the surfaces of the drops are rough and pitted. The anterior surfaces of the button-type australites were shaped during the final descent which did not affect the rough posterior surfaces; see figures 1 and 2. The australites, therefore, were members of the skipping cluster; also, the less compact and uniformly pitted tektites from the strewn fields of Southeast Asia were members of the immediately descending cluster.

In order to illustrate the thickness and the temperature level in the radiatively heated layer in case of the parent meteor with $V_i = 10$ km/sec treated in section Vb, an approximate analysis is carried out which rests on the following assumptions:

(1) the surface temperature T_s is determined by the equation vapor pressure equals external pressure rather than by the vacuum evaporation rate;

(2) the material may be treated as compact and the absorption of heat by the interior boiling process may be neglected.

Fig. 23 shows the temperature profiles $T(z,t)$ °K resulting from this approach along the axis of symmetry of the above mentioned parent meteor at the altitude $H = 85.31$ km for the values $\alpha = 100$, 1000, and ∞ of the absorption coefficient per meter. Because of the large instantaneous equilibrium gas radiation rate of 34,100 kcal/m^2 sec incident at the stagnation point at that time, the true surface temperature T_s exceeds considerably the value $T_s = 2033$ °K. This example verifies that sufficiently high temperatures can be reached over a layer of appreciable thickness; the described disintegration and shaping processes, therefore, are feasible.

The small liquid drops, which are formed by surface tension from the spongy substance, can leave the atmosphere and re-enter as treated in section IV if their exit speed is smaller than 11.2 km/sec. Since skipping drops are released from the parent meteor only during the end of its ascending flight in the atmosphere according to ref. 16, the parent meteor must also possess an exit speed of less than 11.2 km/sec. The trajectory data presented in section Vb for the parent meteor indicates that its entry speed exceeds its exit speed only by a few hundred m/sec. This argument points to the moon as the only possible extraterrestrial origin of the parent meteor flight.

d. Arrival of a Conglomerate of Loosely Bound Stone Bodies

Since solid stone meteors cannot be converted into glass by melting in hypersonic flight, as has been shown, and since glassy meteors are

less likely to arrive at the outer edge of the earth's atmosphere, the possibility of a conglomerate of siliceous gravel and a bonding material like ice should be investigated. Aerodynamic forces dissolve this conglomerate upon its entry into the atmosphere. For the members inside the optically thick cluster, aerodynamic heating together with mutual exchange of radiation causes nearly uniform surface temperatures. Calculations show that the obtainable surface temperatures are smaller than 2000 °K and thus too low for fusion of siliceous rock into glass. Since, also, only spherical bodies of radius ≤ 0.5 cm reach a uniform temperature level in their interiors, this hypothesis of a conglomerate cannot account for the fusion of stone into glass.

CONCLUSIONS

Ablation and trajectory analysis and experiments indicate that an average weight button-type australite entered the atmosphere as a glassy sphere at shallow angles relative to earth's horizon and with entry speeds > 6.5 km/sec in order to experience the observed average figure of more than 70% mass loss by ablation in flight. According to the calculated results and in agreement with observations of natural tektites and experimental results in ref. 9, only a thin layer of solidified melt beneath the final front surface of button-type australites shows a systematic striae deformation. Formation of the final button shapes thus was by aerodynamic heating acting on rigid glass and not by aerodynamic pressure acting on soft glass.

The problems formulated at the end of section I can be answered as follows by employing the results of trajectory and ablation analysis which have just been presented:

(1) Tektite flight could have started at the earth's surface only in the extremely unlikely case that a highly transparent glassy body of $\gg 1700$ tons departs at > 6 km/sec.

(2) Tektites could have been released in flight from a glassy meteor which is sufficiently transparent to thermal radiation. Characteristic features of different groups of tektites can be explained by this hypothesis.

(3) Fusion of siliceous rock into glass by aerodynamic effects is impossible.

Tektites then are remnants of extraterrestrial glassy bodies which entered the earth's atmosphere in skipping flight and, probably, were removed by meteor impact from the moon. Glassy meteors which descend directly or stony meteors cannot release meteorites of well-defined shape like tektites.

Table 1

Comparison of Results for Initially Spherical and Initially Hemispherical Models

Trajectory Parameters			Initially Spherical Model			Initially Hemispherical Model		
V_i	θ_i	R(0)	$m(t_f)/m(0)$	$T_{s,max}$	$\frac{\int v_s dt}{\int v_\infty dt}$	$\frac{m(t_f)}{m(0)}$	$T_{s,max}$	$\frac{\int v_s dt}{\int v_\infty dt}$
km/sec	deg	cm		°K			°K	
10	90	1.3	.767	2415	.530	.713	2366	.537
10	40	1.3	.720	2390	.518	.663	2328	.530
10	10	1.3	.577	2246	.496	.500	2197	.507
8	90	1.3	.802	2385	.444	.767	2300	.467
8	40	1.3	.762	2340	.438	.727	2262	.466
8	10	1.3	.640	2206	.427	.601	2143	.451
7	90	1.3	.828	2336	.392	.805	2258	.424
7	40	1.3	.791	2251	.386	.771	2202	.423
7	10	1.3	.689	2177	.381	.672	2127	.411

Table 2

Interpretation of Figures 5 through 15

Parameter	Symbol and Physical Unit	Figure Number	Increase of Entry Flight Speed V_i	Increase of Entry Flight Angle θ_i in the range $0 \leq \theta_i \leq 30°$	Increase of Entry Mass m(0)	Increase of Vapor Pressure Level
Kinetic Energy Converted into Heat	$\frac{m(0)V_i^2}{2}$ [mkg]		Increase proportional to V_i^2	No Change	Increase Proportional to m(0)	No Change
Relative Mass Loss	$1 - \frac{m(t_f)}{m(0)}$	5 & 6	Moderate Increase	Strong Decrease	Moderate Decrease	Strong Decrease
Horizontal Distance Covered in Flight	D [km]	7	Nearly Constant	Very Strong Decrease	Small Increase	Nearly Constant
Ratio of Aerodynamic Heat Transfer to Kinetic Energy Converted into Heat.	$\frac{\int_0^{t_f} \dot{q}_{aero}(t)dt \left[\frac{kcal}{m^2}\right]}{\frac{m(0)V_i^2}{2A}\left[\frac{mkg}{m^2}\right]\left[\frac{kcal}{427\ mkg}\right]}$	8	Small Increase	Small Decrease		Very Small Increase
Altitude where Maximum of Aerodynamic Heat Pulse Occurs	H* [km]	9	Small Increase	Moderate Decrease	Small Decrease	No Change
Duration of Aerodynamic Heating Pulse	Δt [sec]	10		Strong Decrease	Moderate Increase	No Change
Maximum Surface Temperature	$T_{s,max}$ [°K]	11	Small Increase	Moderate Increase	Moderate Increase	Strong Decrease
Maximum Aerodynamic Heating Rate	$\dot{q}_{aero,max}\left[\frac{kcal}{m^2 sec}\right]$	12	Strong Increase	Strong Increase	Moderate Increase	Very Small Increase

Table 2 (Cont'd)

Interpretation of Figures 5 through 15

Parameter	Symbol and Physical Unit	Figure Number	Increase of Entry Flight Speed V_i	Increase of Entry Flight Angle θ_i in the range $0 \leq \theta_i \leq 30°$	Increase of Entry Mass m(0)	Increase of Vapor Pressure Level
Ratio of Heat Radiated from Surface to Aerodynamic Heating	$\frac{\int_o^{t_f} q_{rad}(t)dt\left[\frac{kcal}{m^2}\right]}{\int_o^{t_f} \bar{q}_{aero}(t)dt\left[\frac{kcal}{m^2}\right]}$	13	Moderate Decrease	Moderate Decrease	Nearly Constant	Strong Decrease
Ratio of Heat Blocked by Mass Transfer Effect to Aerodynamic Heating	$\frac{\int_o^{t_f} q_{bl}(t)dt\left[\frac{kcal}{m^2}\right]}{\int_o^{t_f} \bar{q}_{aero}(t)dt\left[\frac{kcal}{m^2}\right]}$	14	Moderate Increase	Small Increase	Very Small Increase	Strong Increase
Ratio of Evaporation to Total Ablation	$\frac{\int_o^{t_f} v_s(t)dt[mm]}{\int_o^{t_f} v_\infty(t)dt[mm]}$	15	Moderate Increase	Small Increase		Strong Increase

LIST OF REFERENCES

1. Adams, M. C., W. E. Powers, and S. Georgiev, An Experimental and Theoretical Study of Quartz Ablation at the Stagnation Point, AVCO Research Report 57, 1959.

2. Adams, E. W., Analysis of Quartz and Teflon Shields for a Particular Re-Entry Mission, Proceedings of the 1961 Heat Transfer and Fluid Mechanics Institute, Stanford University Press, 1961, pp. 222 - 236.

3. Adams, E. W., A Comparison of Transient and Quasi-Steady Performance of Melting-Type Re-Entry Shields, Journal of the Aerospace Sciences, Vol. 27, Nov. 1960, pp. 791 - 792.

4. Adams, E. W. and R. M. Huffaker, Application of Ablation Analysis to Stony Meteorites and the Tektite Problem, Nature, in press.

5. Baker, G., Tektites, Memoirs of the National Museum of Victoria, Melbourne, 1959.

6. Bethe, H. A. and M. C. Adams, A Theory for the Ablation of Glassy Materials, Journal of the Aerospace Sciences, Vol. 26, June 1959, p. 321.

7. Chao, E. C. T., I. Adler, E. D. Dwornik, and J. Littler, Metallic Spherules in Tektites from Isabela, the Philippines, Science, Jan. 1962, Vol. 135, pp. 97 - 98.

8. Chapman, D. R., Recent Re-Entry Research and the Cosmic Origin of Tektites, Nature, Vol. 188, Oct. 1960, pp. 353 - 355.

9. Chapman, D. R., H. K. Larson, and L. A. Anderson, Aerodynamic Evidence Pertaining to the Entry of Tektites into the Earth's Atmosphere, NASA Technical Report R - 134, Washington, January 1962.

10. Eckert, E. R. G. and R. M. Drake, Jr., Heat and Mass Transfer, McGraw-Hill Book Co., New York, London, Toronto, 1959.

11. Fenner, C., Trans. Roy. Soc. S. Australia, 62: 208, Part II, 1938.

12. Grant, K., Proceedings Roy. Soc. Victoria, Vol. 21 (2), 1909, pp. 444 - 448.

13. Hanuš, F., Rozpravy II Třídy Čes Akademie Roč, XXXVII, čís 24, 1958.

14. Hardcastle, H., New Zealand J. Science and Technol., 8:65, 1926.

15. O'Keefe, J. A., The Origin of Tektites, NASA Techn. Note D-490, Washington, Nov. 1960.

LIST OF REFERENCES (CONT'D)

16. O'Keefe, J. A. and B. E. Shute, Tektites and Natural Satellites of the Earth, Aerospace Engineering, July 1960, p. 26.

17. Öpik, E. J., Physics of Meteor Flight in the Atmosphere, Interscience Publishers, Inc., New York, 1958.

18. Öpik, E. J., The Survival of Stray Bodies in the Solar System, Annales Academiae Scientiarium Fennicae, Series A, III Geologica-Geographica, 61, Helsinki, 1961.

19. Oswald, J., Meteorické Sklo, Praze:Nákladem České Akademie věd a Umění, 1942.

20. Schick, H. L., Analysis of some of the Physical and Chemical Properties of Silica (SiO_2) of Importance in Ablation Behavior, AVCO Report RAD-TR-2-59-6.

21. Urey, H. C., Origin of Tektites, Nature, Vol. 179, 1957, p. 556.

22. Viste, E. and E. Anders, Cosmic-Ray Exposure History of Tektites, The University of Chicago, The Enrico Fermi Institute for Nuclear Studies, Report EFINS 61-66, 1961.

23. Volarovich, M. P. and A. A. Leontieva, C. R. (Doklady) Acad. Sci. U.S.S.R., Vol. 22, 1939.

24. Wing, L. D., Radiative Heat Transfer to Hemispheric Noses, Journal of the American Rocket Society, Dec. 1961, pp. 90 - 92.

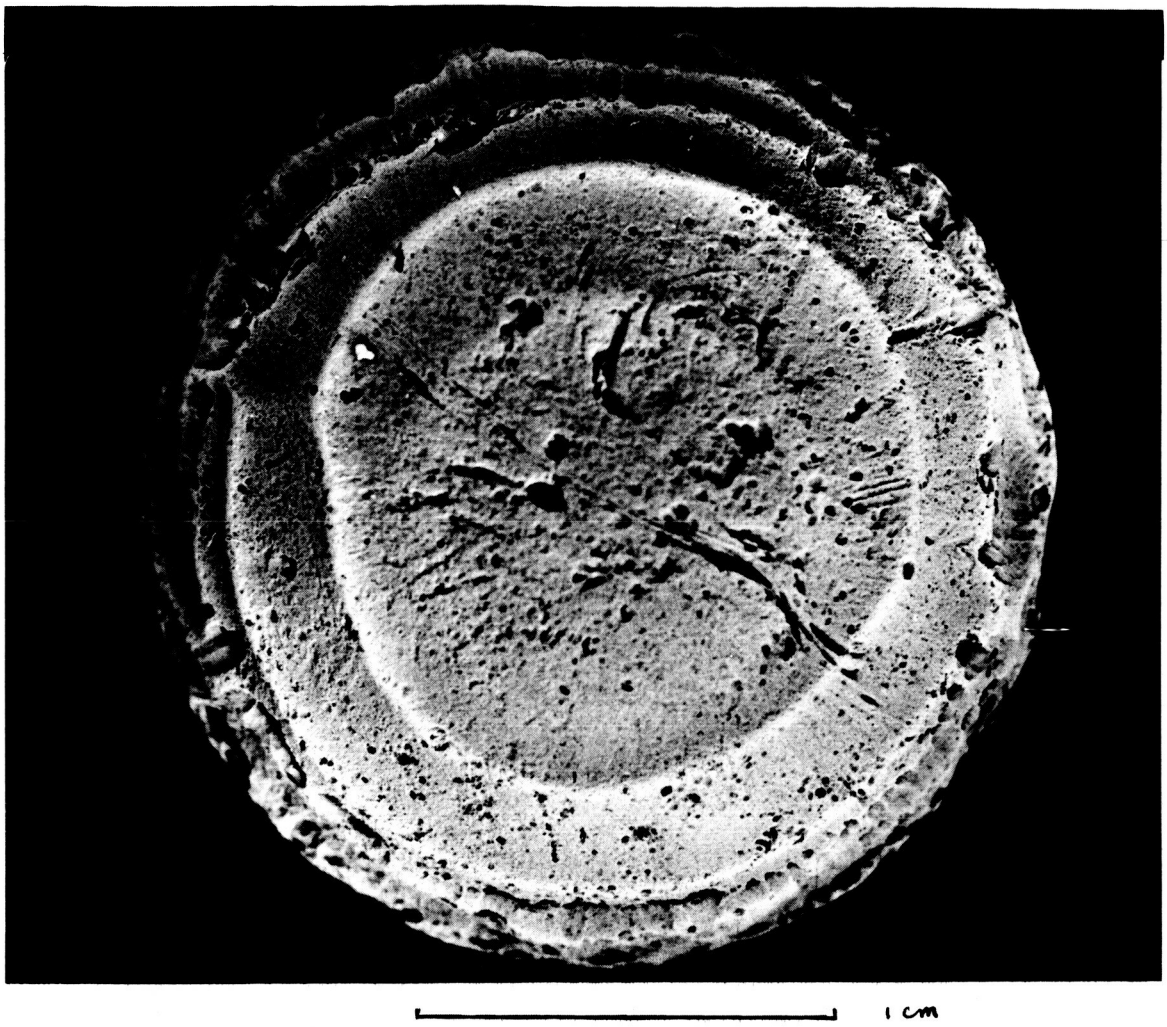

This photograph was made available through the courtesy of the Smithsonian Institute, Washington, D. C.

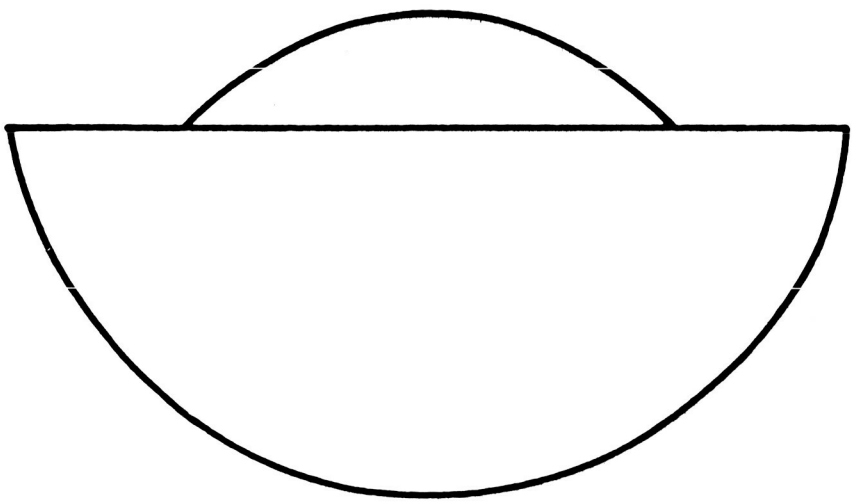

FIG. 1. ANTERIOR SURFACE AND CROSS SECTION OF BUTTON-TYPE AUSTRALITE.

This photograph was made available through the courtesy of the Smithsonian Institute, Washington, D. C.

FIG. 2. POSTERIOR SURFACE OF BUTTON-TYPE AUSTRALITE.

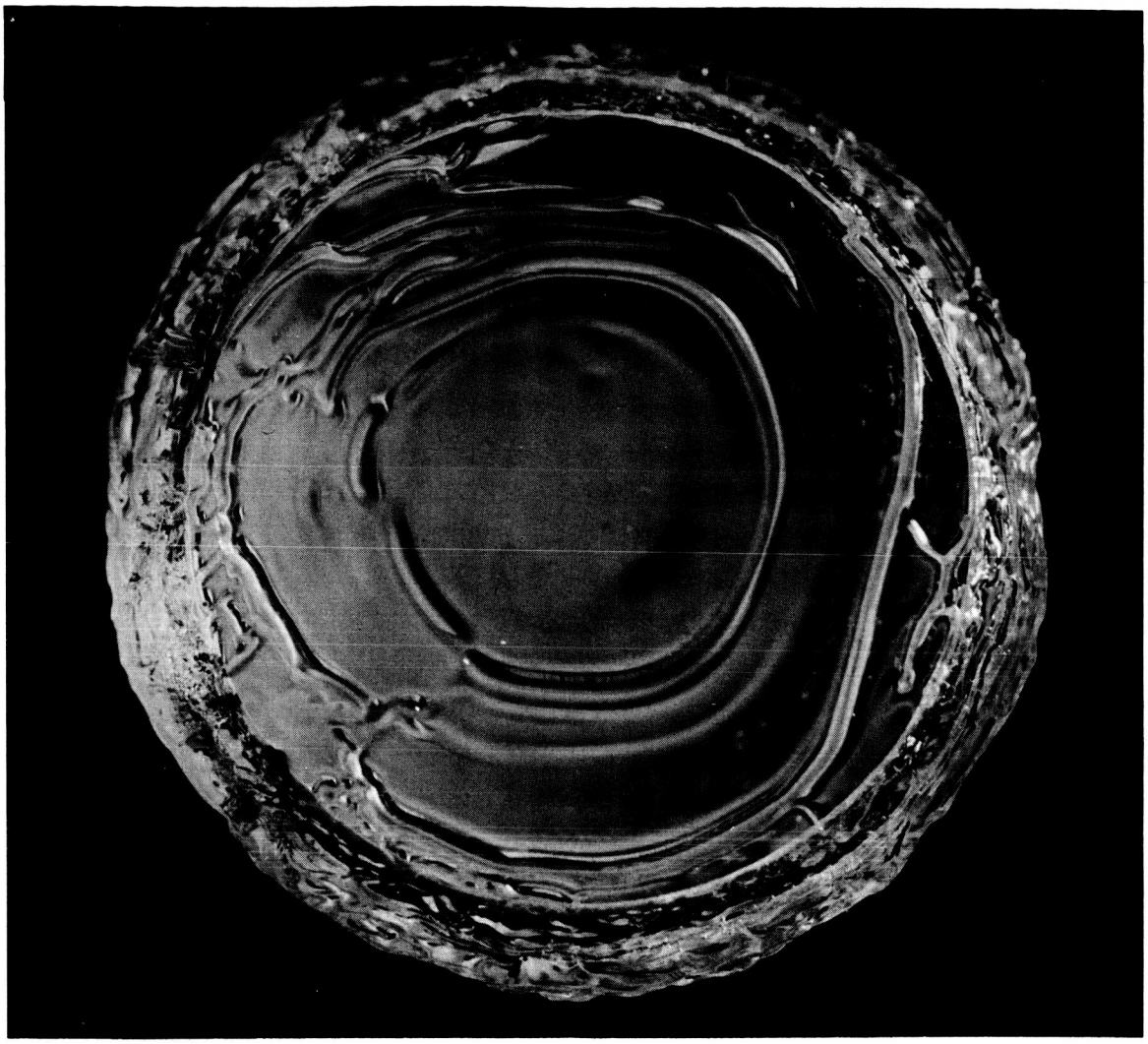

This photograph was made available through the courtesy of Dr. J. A. O'Keefe, Goddard Space Flight Center.

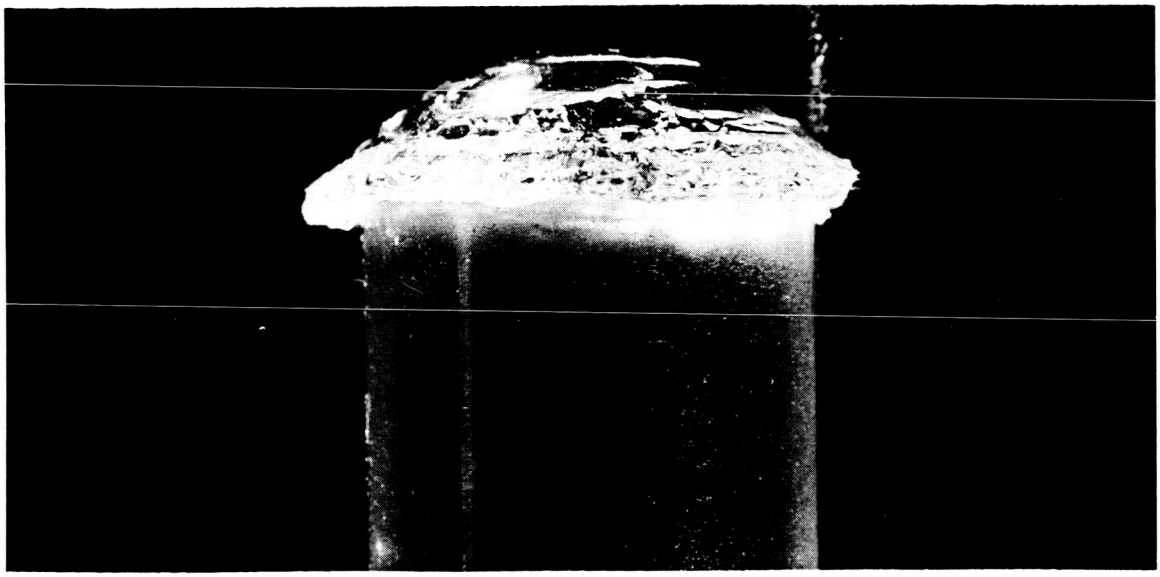

FIG. 3. GLASS ROD ABLATED IN AN ARC-JET FACILITY.

The ablation process is investigated along the axis S_0-O. S_0 = stagnation point before ablation begins; S(t) = stagnation point during and after the end of the ablation period. Ablation is assumed to convert the hemispherical shape A-S_0-B-O-A into the section A-S(t)-B-O-A of a sphere.

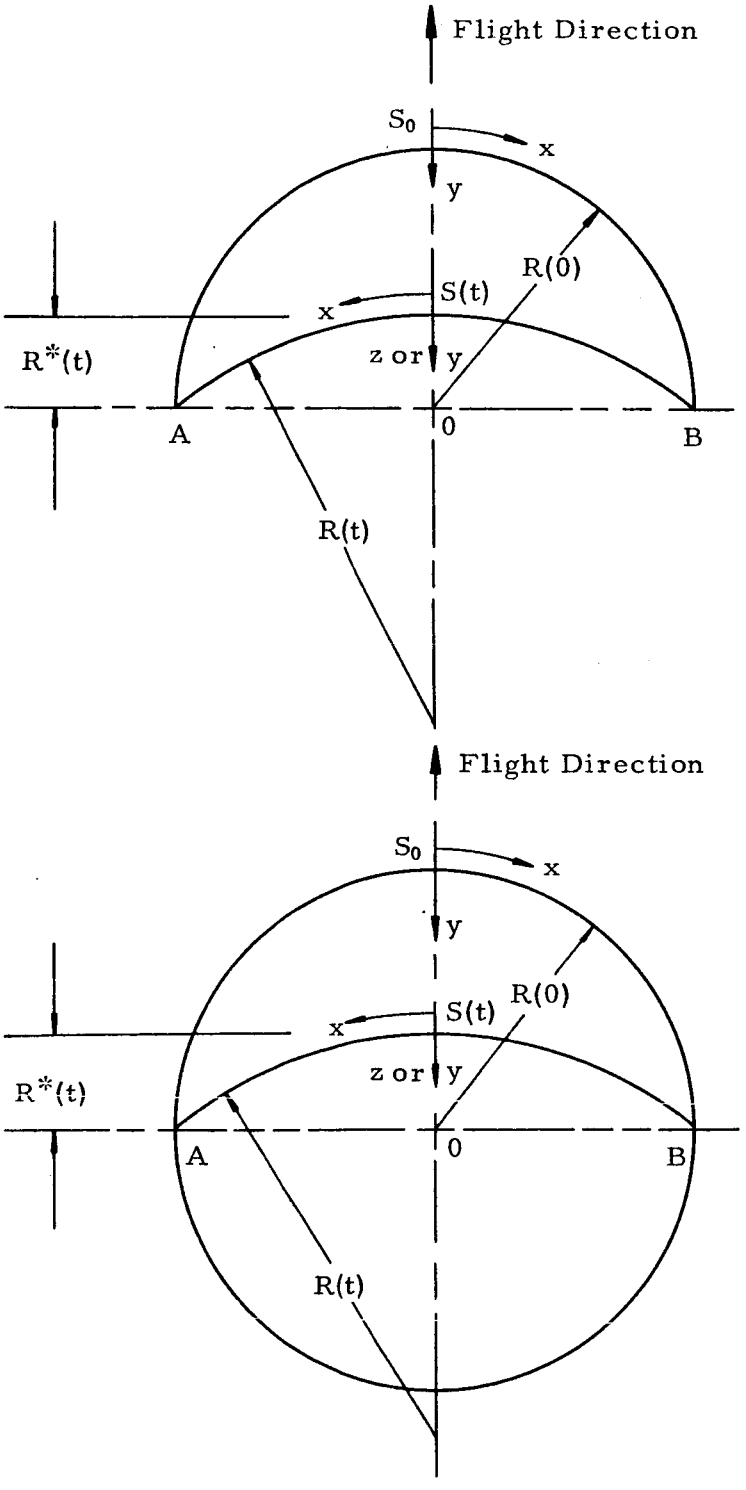

FIG. 4. GEOMETRIES OF INITIALLY HEMISPHERICAL AND SPHERICAL MODELS OF BUTTON-TYPE AUSTRALITES

Data pertains to vapor pressure function $p_{vl}(T)$ and initially hemispheric model with mass m(0):
Radius R(0) = 1.30 cm, i.e. W(0) = 11.04 grams (———)
Radius R(0) = 0.65 cm, i.e. W(0) = 1.38 grams (– – – –)
$m(t_f)$ = final mass at impact time

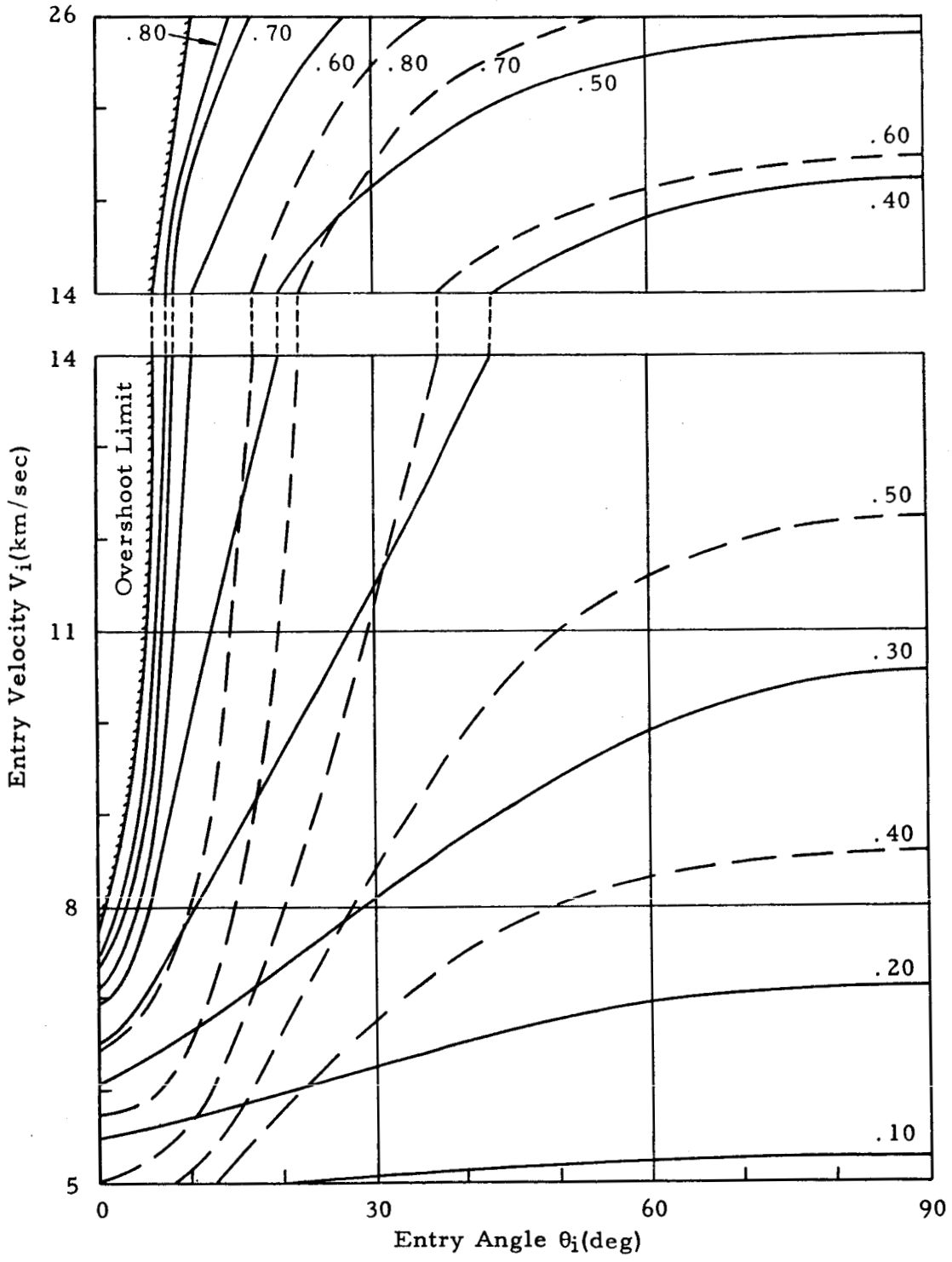

FIG. 5. RELATIVE MASS LOSS, $1 - m(t_f)/m(0)$

Data pertains to initially hemispheric model with mass m(0), radius R(0) = 1.30 cm, i.e. W(0) = 11.04 grams:
Vapor pressure function $p_{v1}(T)$ (———)
Vapor pressure function $p_{v2}(T)$ (— · —)
$m(t_f)$ = final mass at impact time

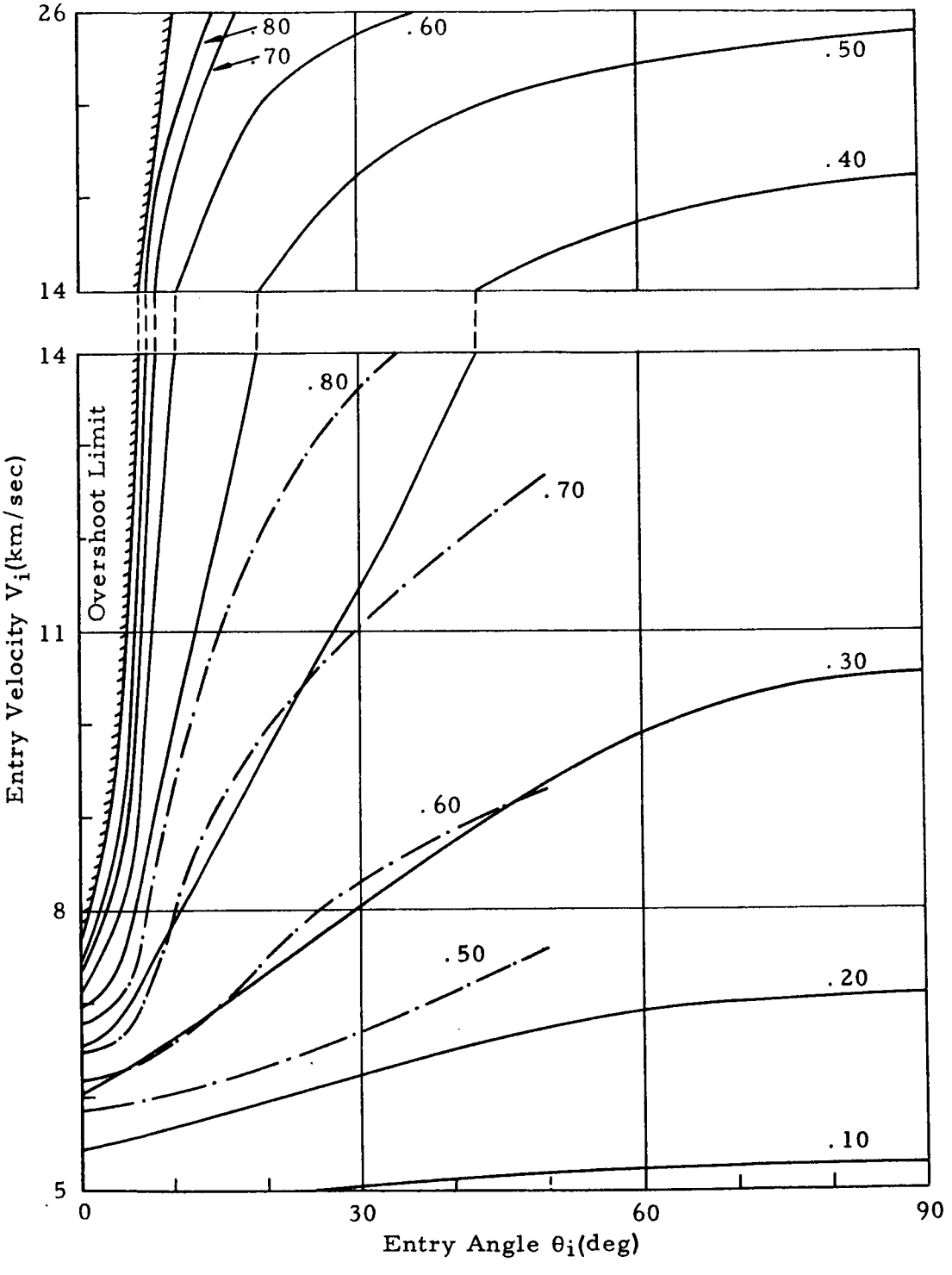

FIG. 6. RELATIVE MASS LOSS, $1 - m(t_f)/m(0)$

Data pertains to vapor pressure function $p_{v1}(T)$ and initially hemispheric model with:
Radius R(0) = 1.30 cm, i.e. W(0) = 11.04 grams (———)
Radius R(0) = 0.65 cm, i.e. W(0) = 1.38 grams (– – – –)

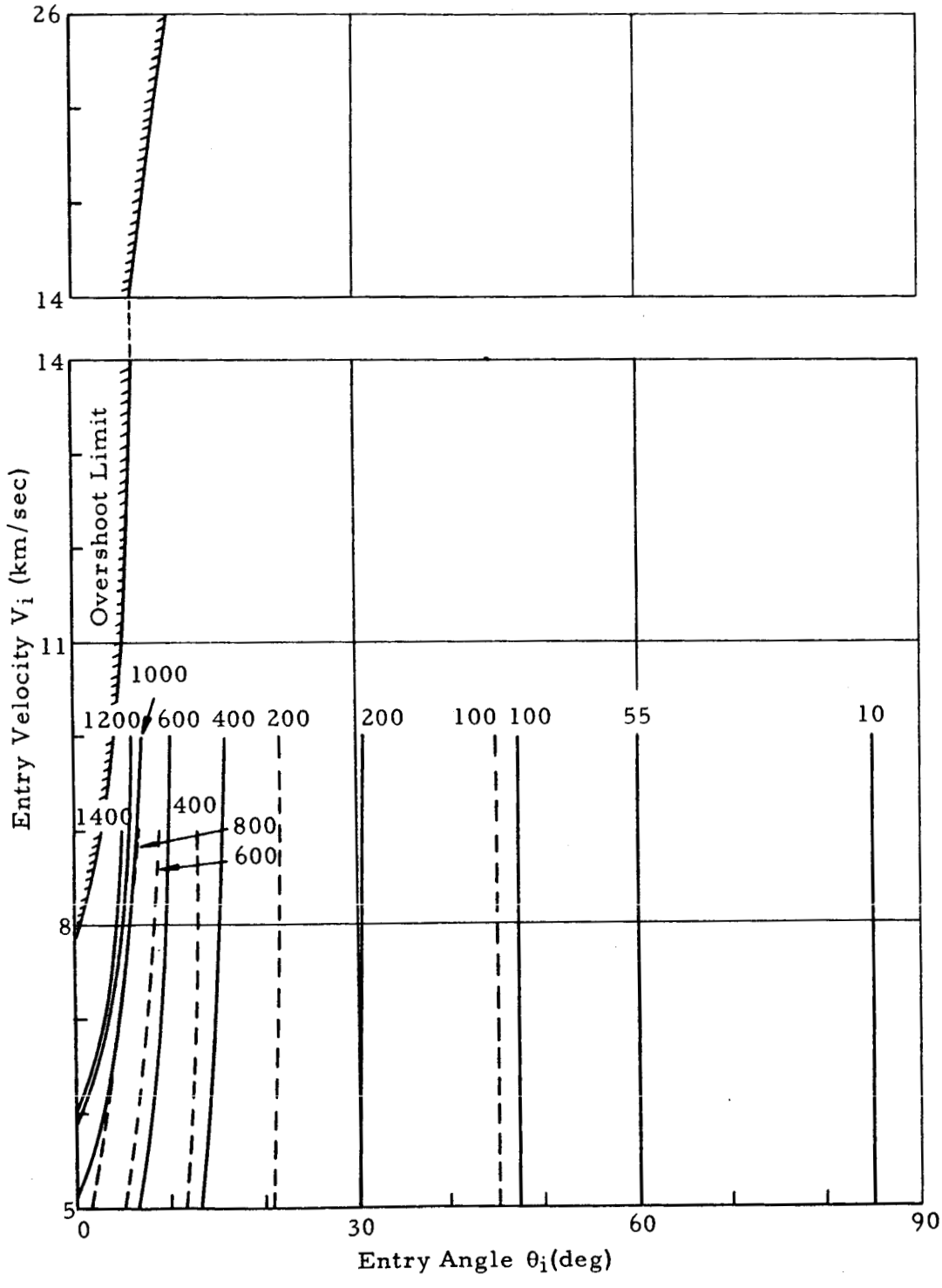

FIG. 7. HORIZONTAL DISTANCE D(t)(KM)COVERED IN FLIGHT

Data pertains to initially hemispheric model with radius R(0) = 1.30 cm, i.e. W(0) = 11.04 grams, and vapor pressure function $p_{v1}(T)$.

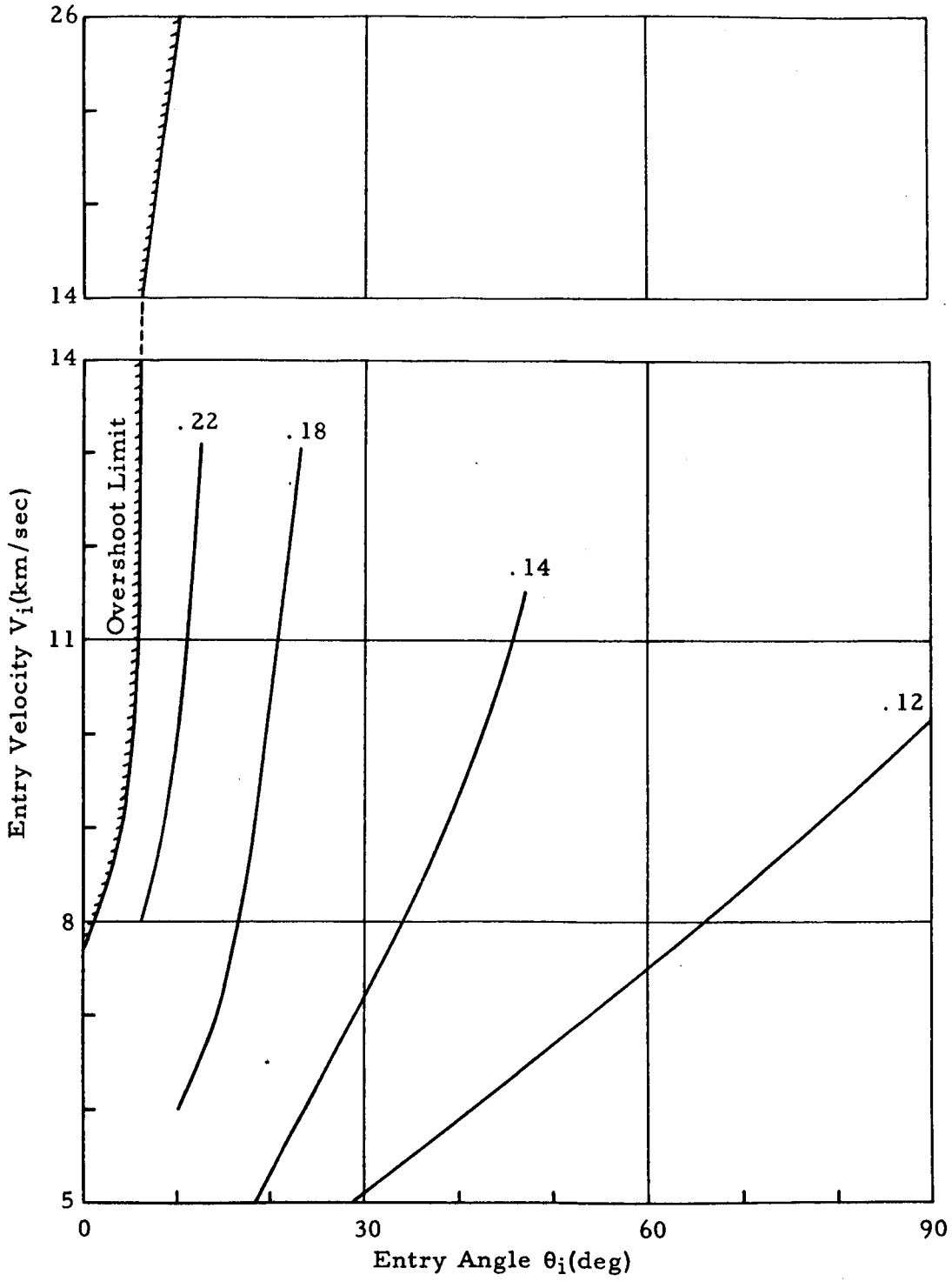

FIG. 8. RATIO OF AERODYNAMIC HEAT TRANSFER AT THE STAGNATION POINT TO KINETIC ENERGY CONVERTED INTO HEAT, $\frac{\int_o^{t_f} \bar{q}_{aero}\, dt}{m(0)V_i^2/2A}$

Data pertains to vapor pressure $p_{vl}(T)$ and initially hemispheric model with:
Radius R(0) = 1.30 cm, i.e. W(0) = 11.04 grams (———)
Radius R(0) = 0.65 cm, i.e. W(0) = 1.38 grams (– – – –)

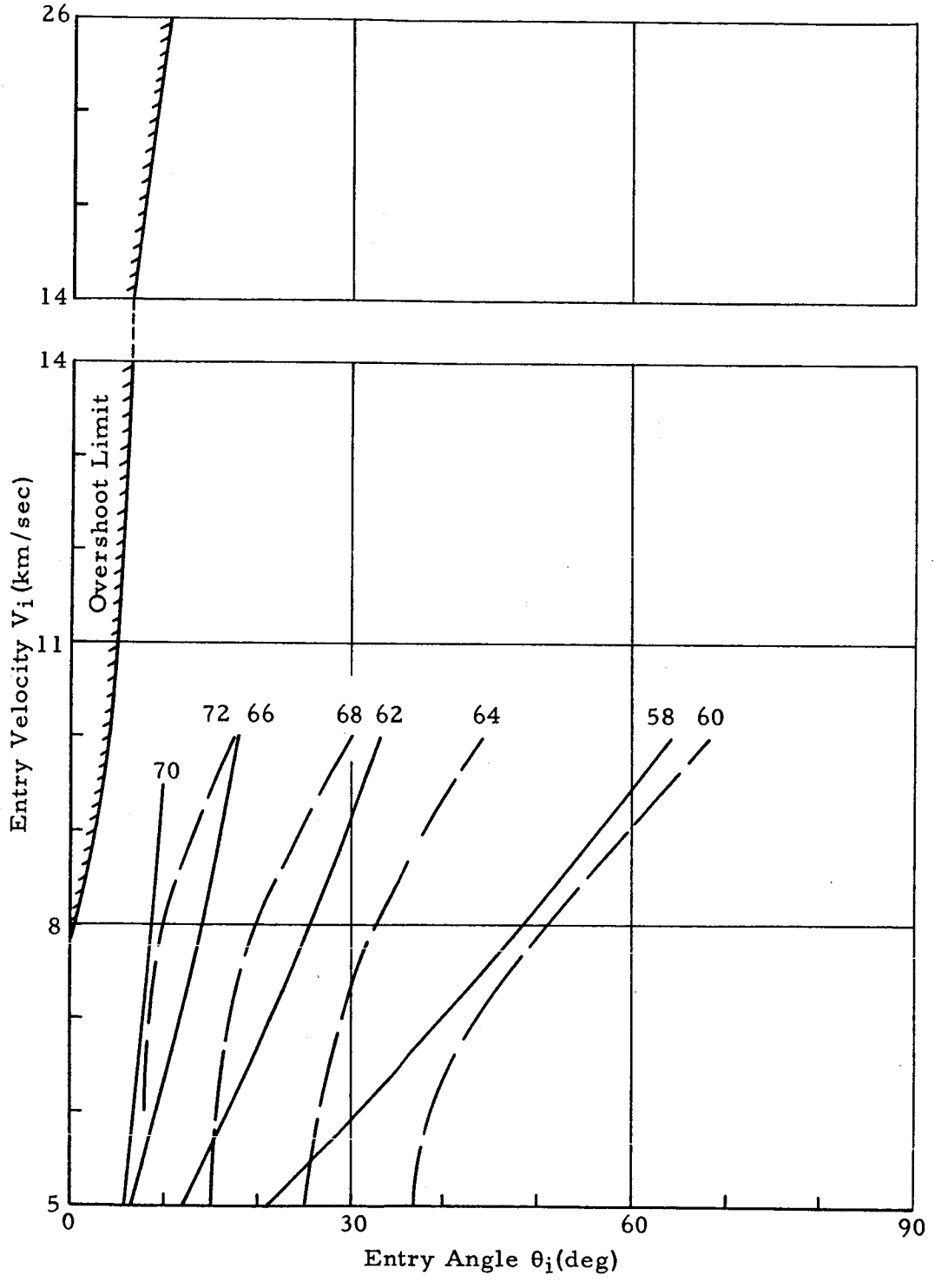

FIG. 9. ALTITUDE H(KM) OF MAXIMUM AERODYNAMIC HEAT TRANSFER AT THE STAGNATION POINT

Data pertains to vapor pressure $p_{v1}(T)$ and initially hemispheric model with:
Radius R(0) = 1.30 cm, i.e. W(0) = 11.04 grams (———)
Radius R(0) = 0.65 cm, i.e. W(0) = 1.38 grams (– – – –)

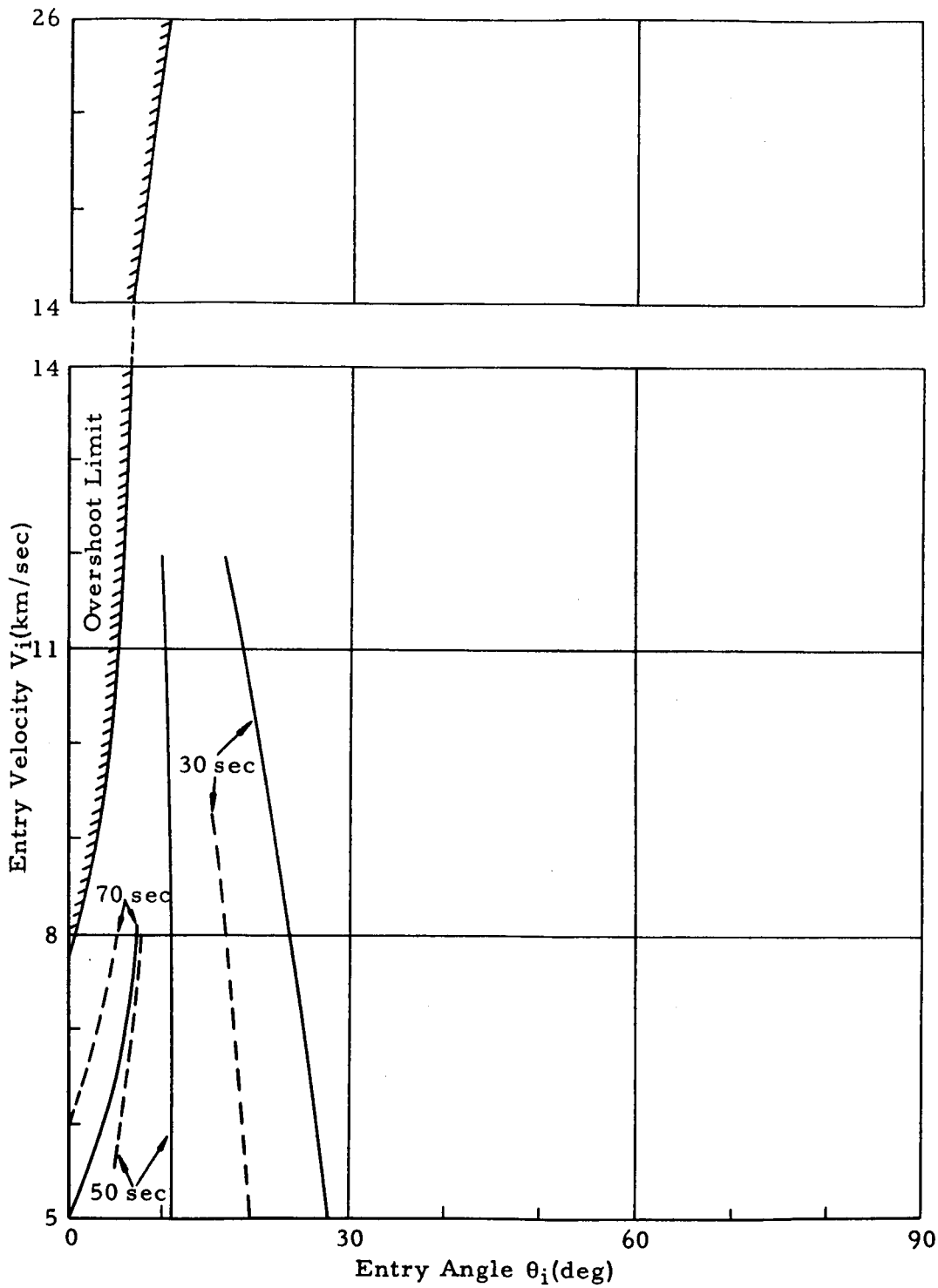

FIG. 10. DURATION OF AERODYNAMIC HEAT TRANSFER PULSE AT THE STAGNATION POINT

Data pertains to initially hemispheric model with:
Radius R(0) = 1.30 cm, i.e. W(0) = 11.04 grams, and vapor pressure $p_{V1}(T)$ (———)
Radius R(0) = 0.65 cm, i.e. W(0) = 1.38 grams, and vapor pressure $p_{V1}(T)$ (– – – –)
Radius R(0) = 1.30 cm, i.e. W(0) = 11.04 grams, and vapor pressure $p_{V2}(T)$ (—·—)

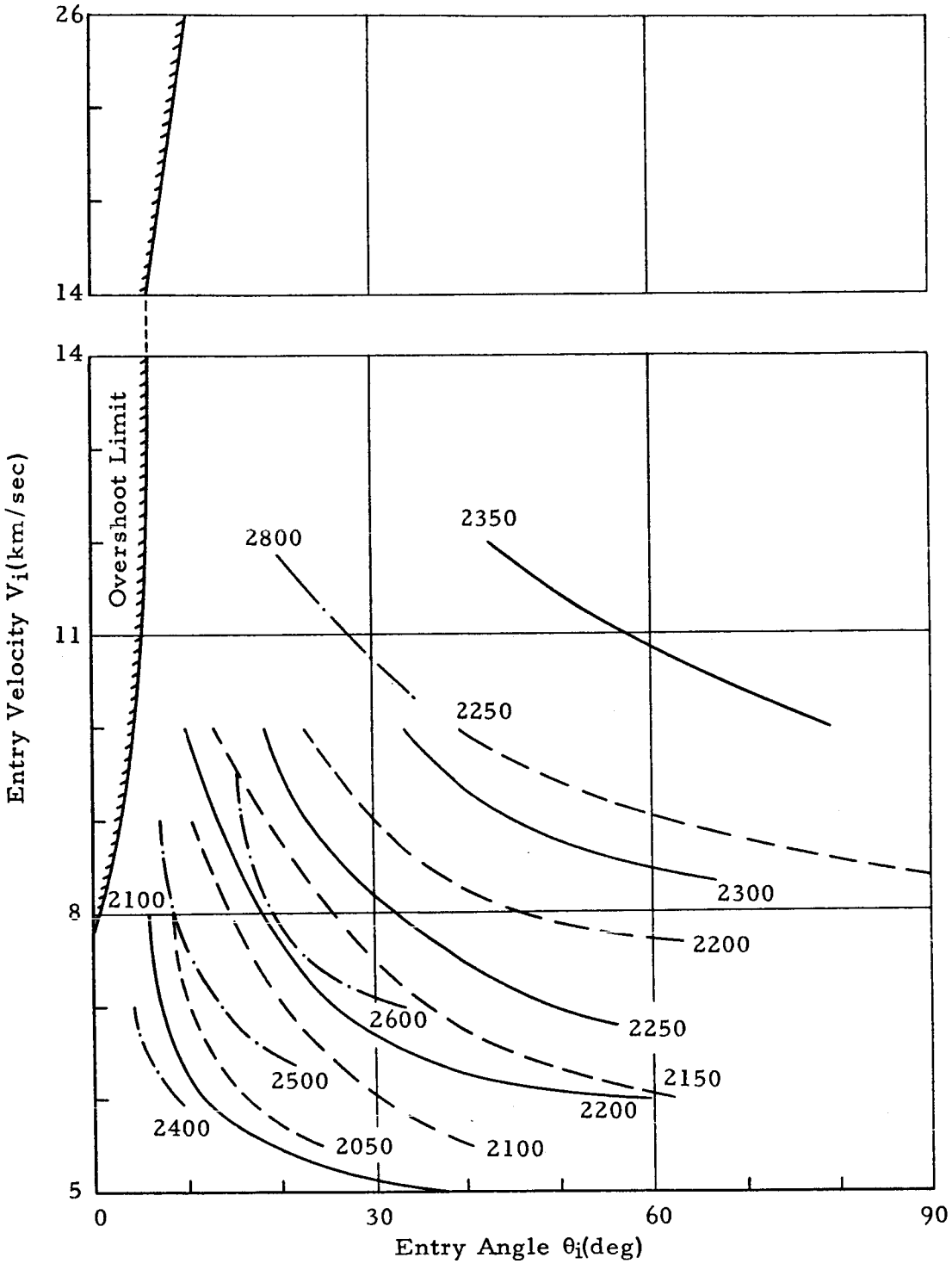

FIG. 11. MAXIMUM SURFACE TEMPERATURE $T_{s,max}$ (°K) AT THE STAGNATION POINT

Data pertains to vapor pressure $p_{v1}(T)$ and initially hemispheric model with:
Radius R(0) = 1.30 cm, i.e. W(0) = 11.04 grams (———)
Radius R(0) = 0.65 cm, i.e. W(0) = 1.38 grams (– – – –)

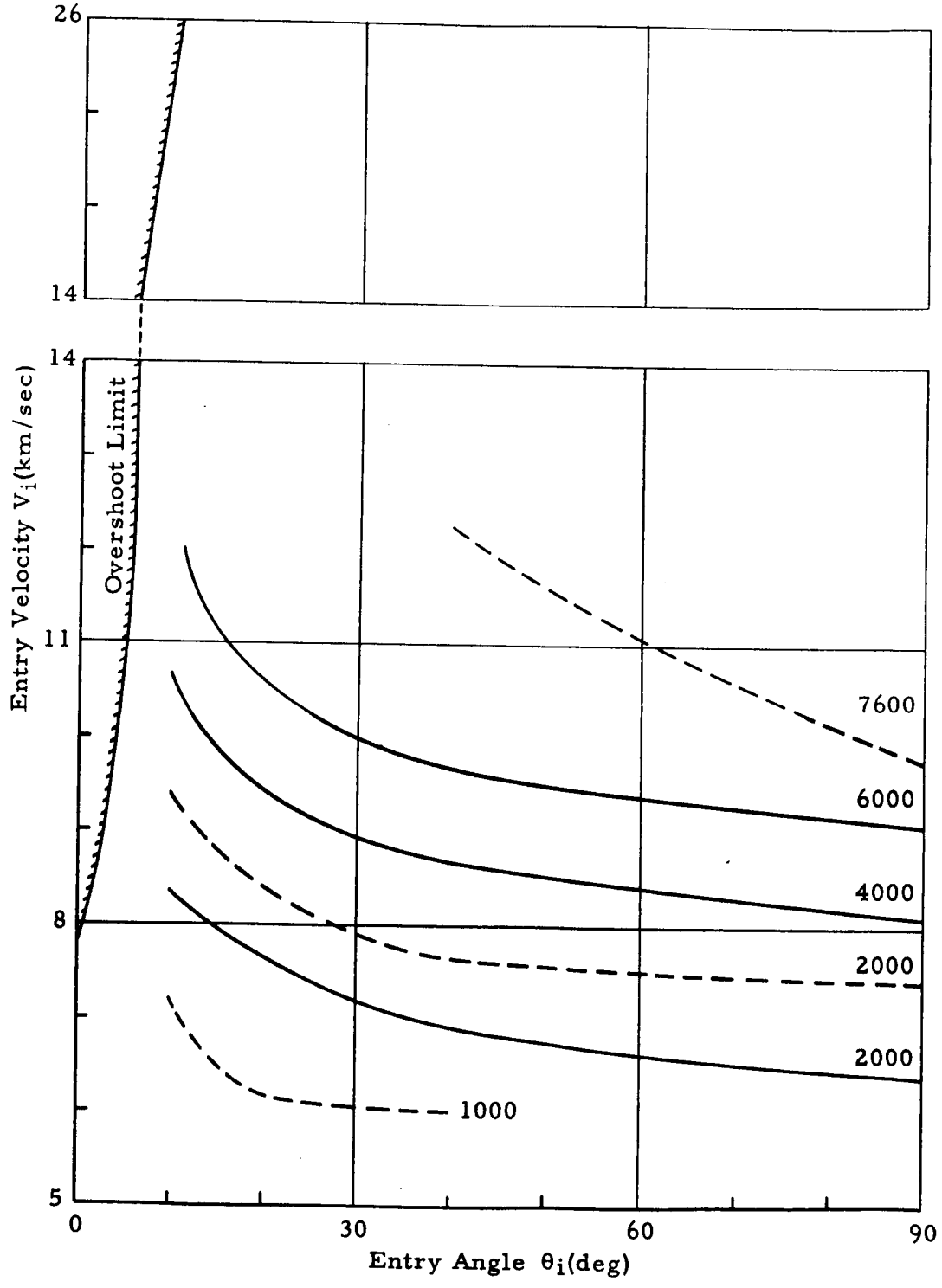

FIG. 12. MAXIMUM AERODYNAMIC HEAT TRANSFER $\bar{q}_{aero,\,max}$ (kcal/m^{2}sec) AT THE STAGNATION POINT

Data pertains to initially hemispheric model with:
Radius R(0) = 1.30 cm, i.e. W(0) = 11.04 grams, and vapor pressure $p_{v1}(T)$ (———)
Radius R(0) = 0.65 cm, i.e. W(0) = 1.38 grams, and vapor pressure $p_{v1}(T)$ (– – – –)
Radius R(0) = 1.30 cm, i.e. W(0) = 11.04 grams, and vapor pressure $p_{v2}(T)$ (—·—)

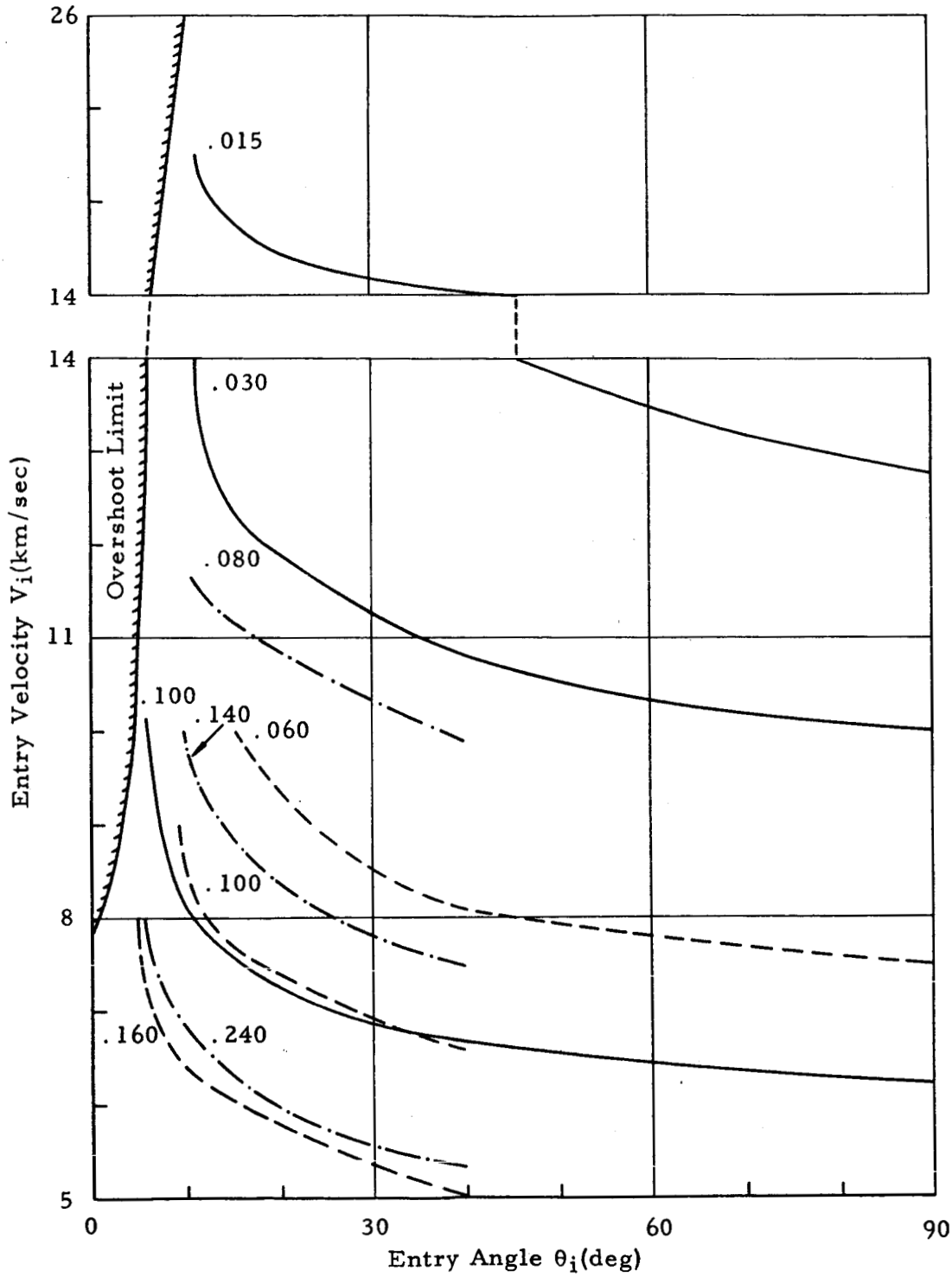

FIG. 13. RATIO OF HEAT RADIATED FROM SURFACE TO AERODYNAMIC HEATING, $\int_0^{t_f} \dot{q}_{rad}\,dt \Big/ \int_0^{t_f} \bar{q}_{aero}\,dt$, AT THE STAGNATION POINT

Data pertains to initially hemispheric model with:
Radius R(0) = 1.30 cm, i.e. W(0) = 11.04 grams, and vapor pressure $p_{v1}(T)$ (———)
Radius R(0) = 0.65 cm, i.e. W(0) = 1.38 grams, and vapor pressure $p_{v1}(T)$ (– – – –)
Radius R(0) = 1.30 cm, i.e. W(0) = 11.04 grams, and vapor pressure $p_{v2}(T)$ (—·—)
$q_{bl} = (\bar{q}_{aero} - q_{aero}) + \gamma h_v V_s$, where $\bar{q}_{aero} - q_{aero}$ is due to the diffusion of vapor across the boundary layer and $\gamma h_v V_s$ is the heat absorbed by the evaporation process.

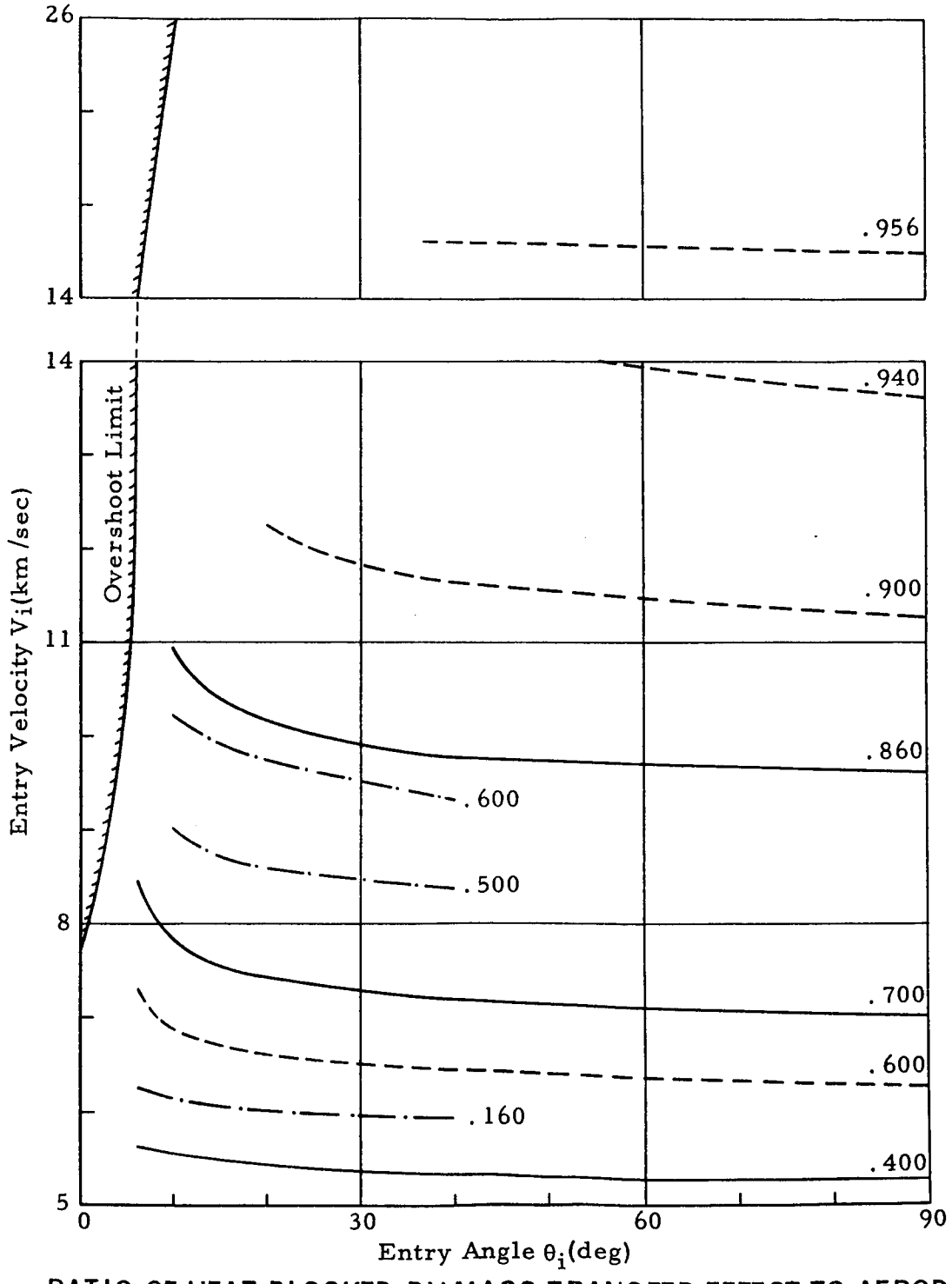

FIG. 14. RATIO OF HEAT BLOCKED BY MASS TRANSFER EFFECT TO AERODYNAMIC HEATING, $\int_0^{t_f} q_{bl}\,dt \Big/ \int_0^{t_f} \bar{q}_{aero}\,dt$, AT THE STAGNATION POINT

Data pertains to initially hemispheric model with:
Radius R(0) = 1.30 cm, i.e. W(0) = 11.04 grams, and vapor pressure $p_{v1}(T)$ (———)
Radius R(0) = 0.65 cm, i.e. W(0) = 1.38 grams, and vapor pressure $p_{v1}(T)$ (– – –)
Radius R(0) = 1.30 cm, i.e. W(0) = 11.04 grams, and vapor pressure $p_{v2}(T)$ (—·—)

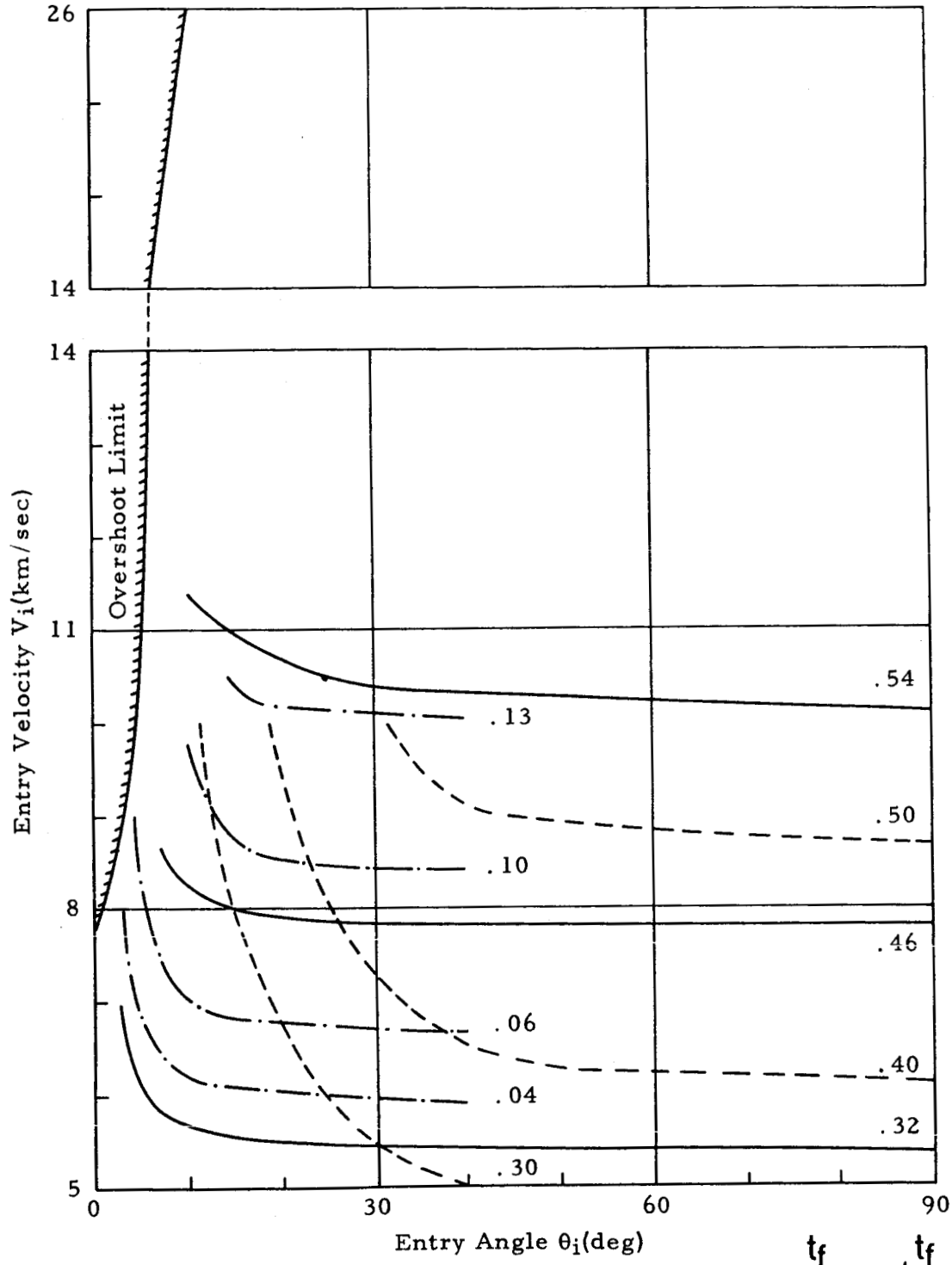

FIG. 15. RATIO OF EVAPORATION TO TOTAL ABLATION, $\int_0^{t_f} V_s\,dt \Big/ \int_0^{t_f} V_\infty\,dt$, AT THE STAGNATION POINT

Data pertains to the particular tektite flight treated in Figures 16 - 21 and the vapor pressure $p_{v1}(T)$. The model initially is a hemisphere with radius R(0) = 1.30 cm, i.e. W(0) = 11.04 grams. Presented functions:
Flight altitude H (———)
Horizontal distance D covered in flight (– – – –)
Flight Mach number M (—·—)

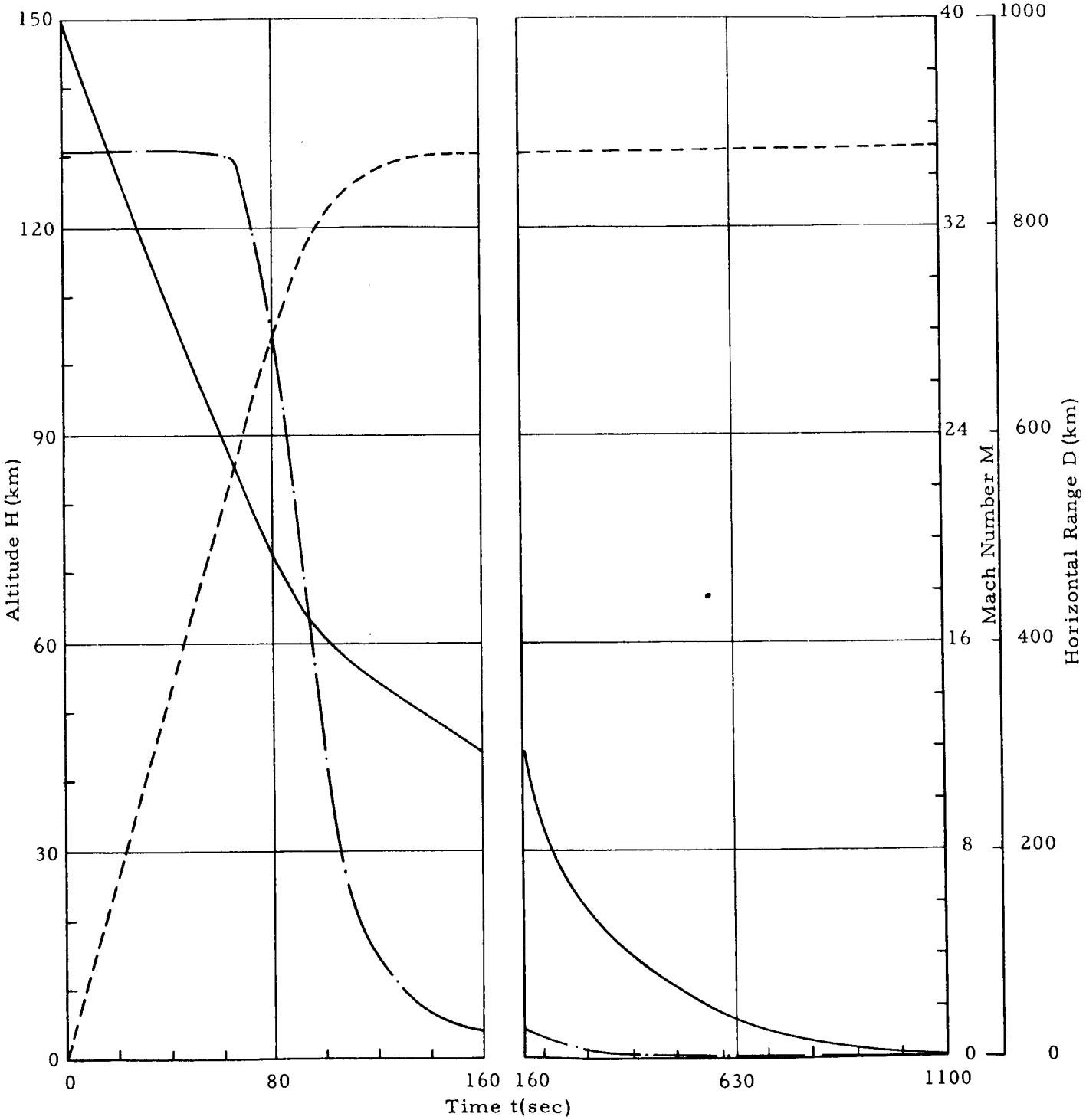

FIG. 16. FLIGHT ALTITUDE, HORIZONTAL DISTANCE, AND MACH NUMBER FOR PARTICULAR TEKTITE TRAJECTORY

Data pertains to the particular tektite flight treated in Figures 16 - 21 and the vapor pressure $p_{v1}(T)$. The model initially is a hemisphere with radius R(0) = 1.30 cm, i.e. W(0) = 11.04 grams. Presented functions:

Flight speed V (———)
Acceleration a (– – – –)
Trajectory angle θ relative to earth's horizontal (—·—)

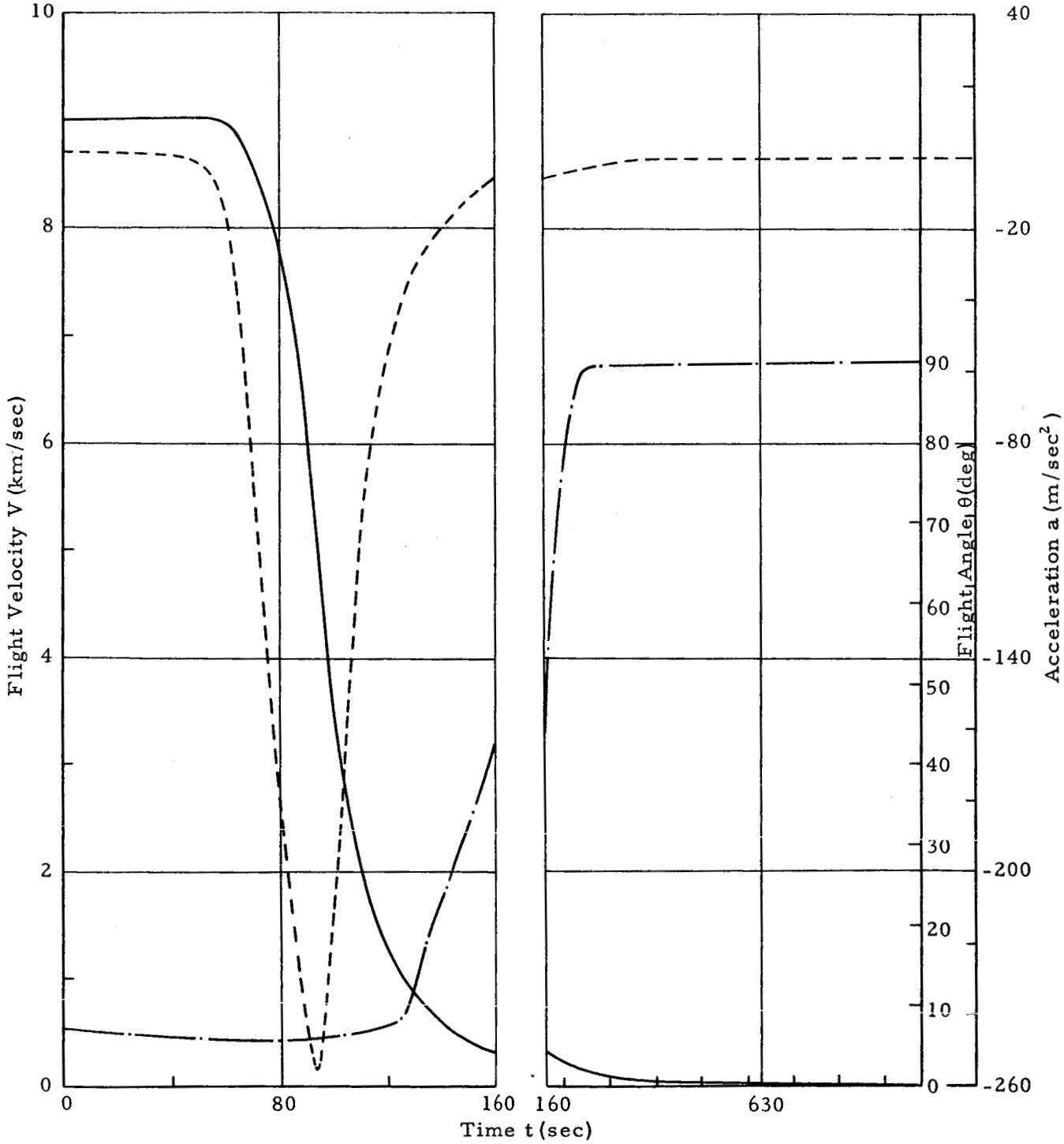

FIG. 17. FLIGHT SPEED, ACCELERATION, AND TRAJECTORY ANGLE FOR PARTICULAR TEKTITE TRAJECTORY

Data pertains to the particular tektite flight treated in Figures 16 - 21 and the vapor pressure $p_{v1}(T)$. The model initially is a hemisphere with radius R(0) = 1.30 cm, i.e. W(0) = 11.04 grams. Presented functions:
aerodynamic heat transfer rate $\bar{q}_{aero}$ to a non-evaporating surface (———), aerodynamic heat transfer rate q_{aero} to the evaporating surface (– – – –), heat radiated from surface, q_{rad} (– · – · –), heat blocked by mass transfer effect, q_{bl}, see legend of Fig. 14, (— — —), and surface temperature T_s (— · · —), all at the stagnation point.

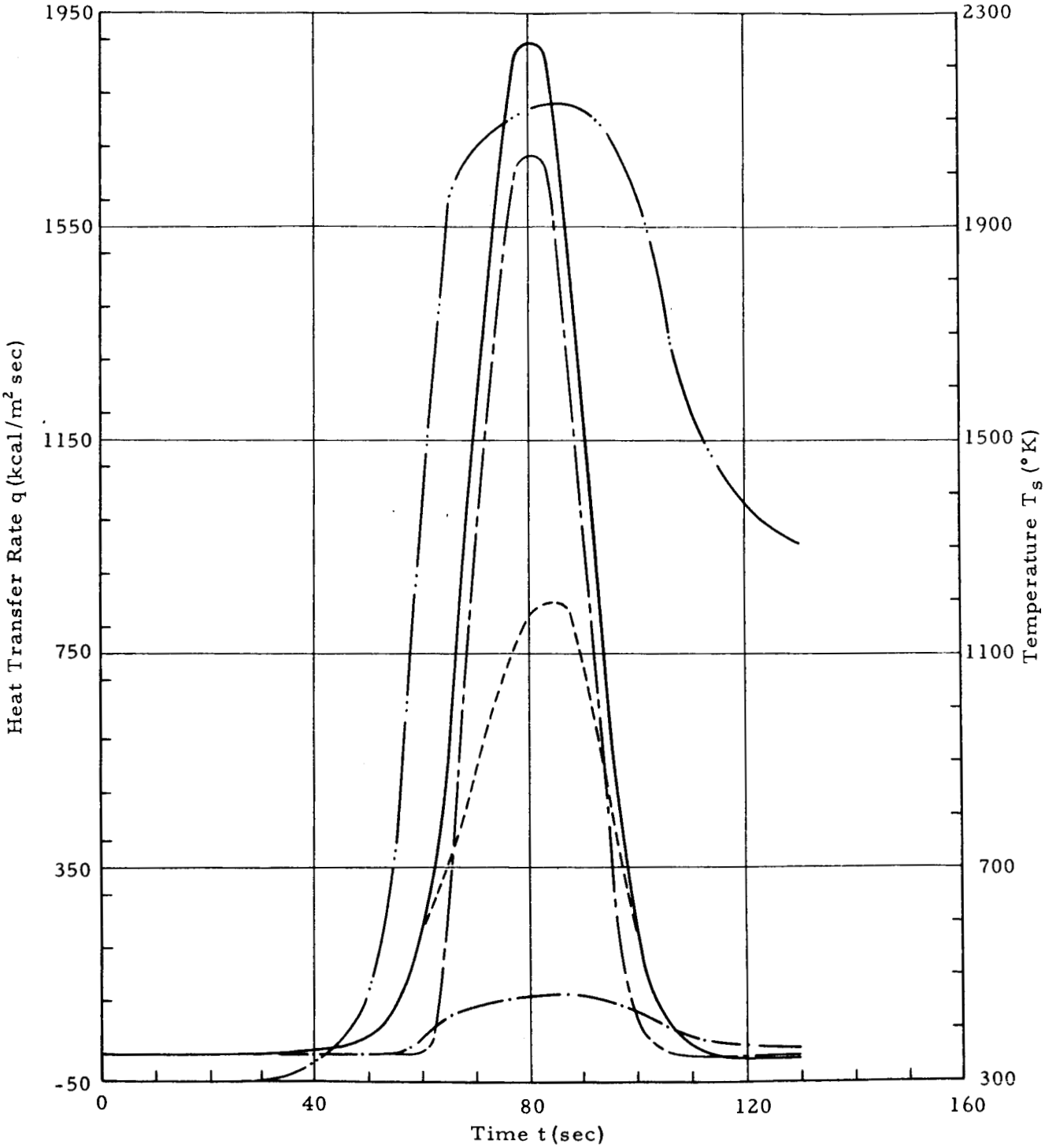

FIG. 18. HEAT FLOW RATES AND SURFACE TEMPERATURE FOR PARTICULAR TEKTITE TRAJECTORY

Data pertains to the particular tektite flight treated in Figures 16 - 21 and the vapor pressure $p_{v1}(T)$. The model initially is a hemisphere with radius R(0) = 1.30 cm, i.e. W(0) = 11.04 grams. Presented functions:

Evaporation speed v_s of the liquid at the surface (———)
Thickness R^* of the model, see Fig. 4, (– – – –)
Mass ratio m(t)/m(0) of model (—·—)
Gradient du/dx of tangential velocity component of melt (—··—)
All at the stagnation point.

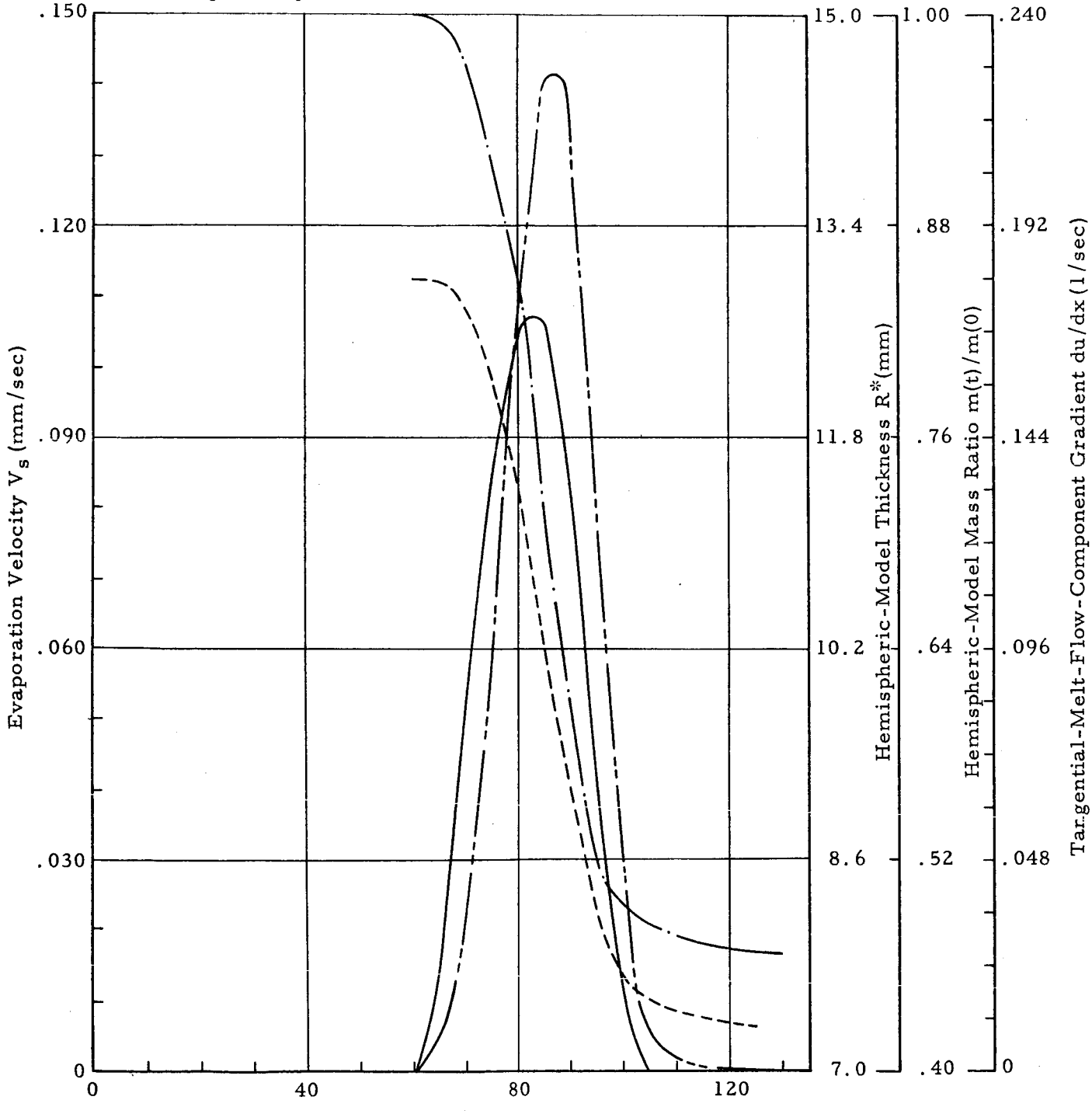

FIG. 19. ABLATION PARAMETERS FOR PARTICULAR TEKTITE TRAJECTORY

Data pertains to the particular tektite flight treated in Figures 16 - 21 and the vapor pressure $p_{v1}(T)$. The model initially is a hemisphere with radius R(0) = 1.30 cm, i.e. W(0) = 11.04 grams. The shaded lines adjacent to the instantaneous locations of the stagnation point indicate the thicknesses of the melt layer.

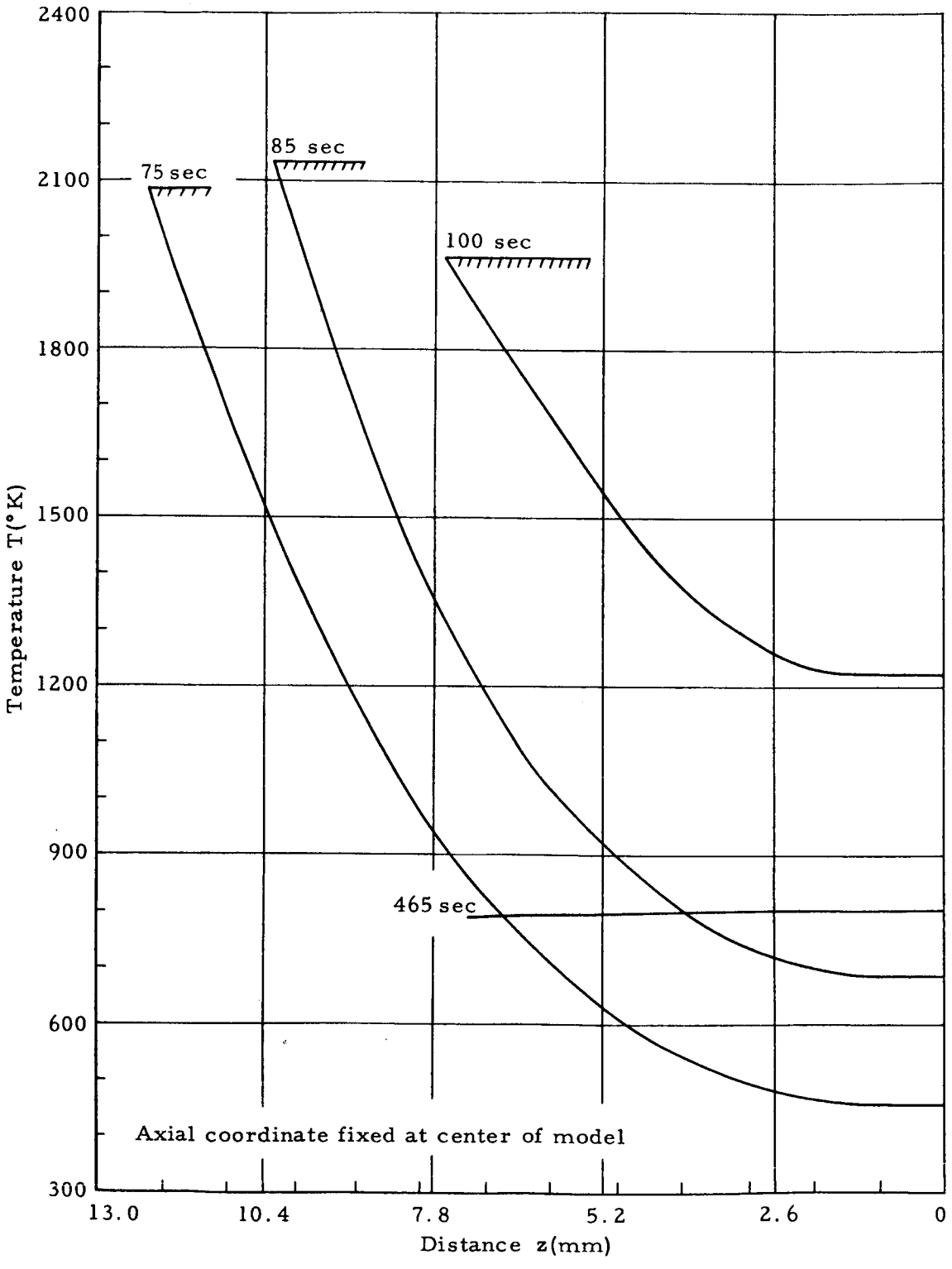

FIG. 20. TEMPERATURE DISTRIBUTION ALONG AXIS FOR PARTICULAR TEKTITE TRAJECTORY

Data pertains to initially hemispheric model with radius R(0) = 1.30 cm, i.e. W(0) = 11.04 grams, entry speed V_i = 9 km/sec, entry angle θ_i = 7°, and vapor pressure $p_{V1}(T)$.

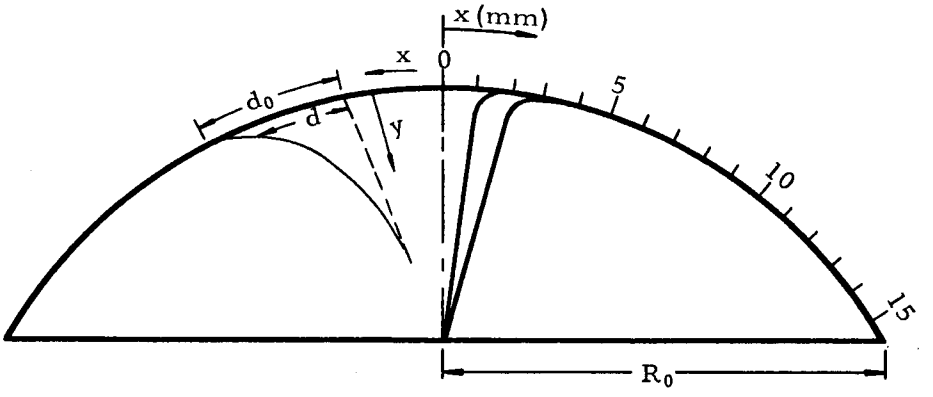

Fig. 21a. Striae After Solidification of Melt

Fig. 21c. Striae Distortion as a Function of y

Fig. 21b. Striae Distortion at the Surface as a Function of x

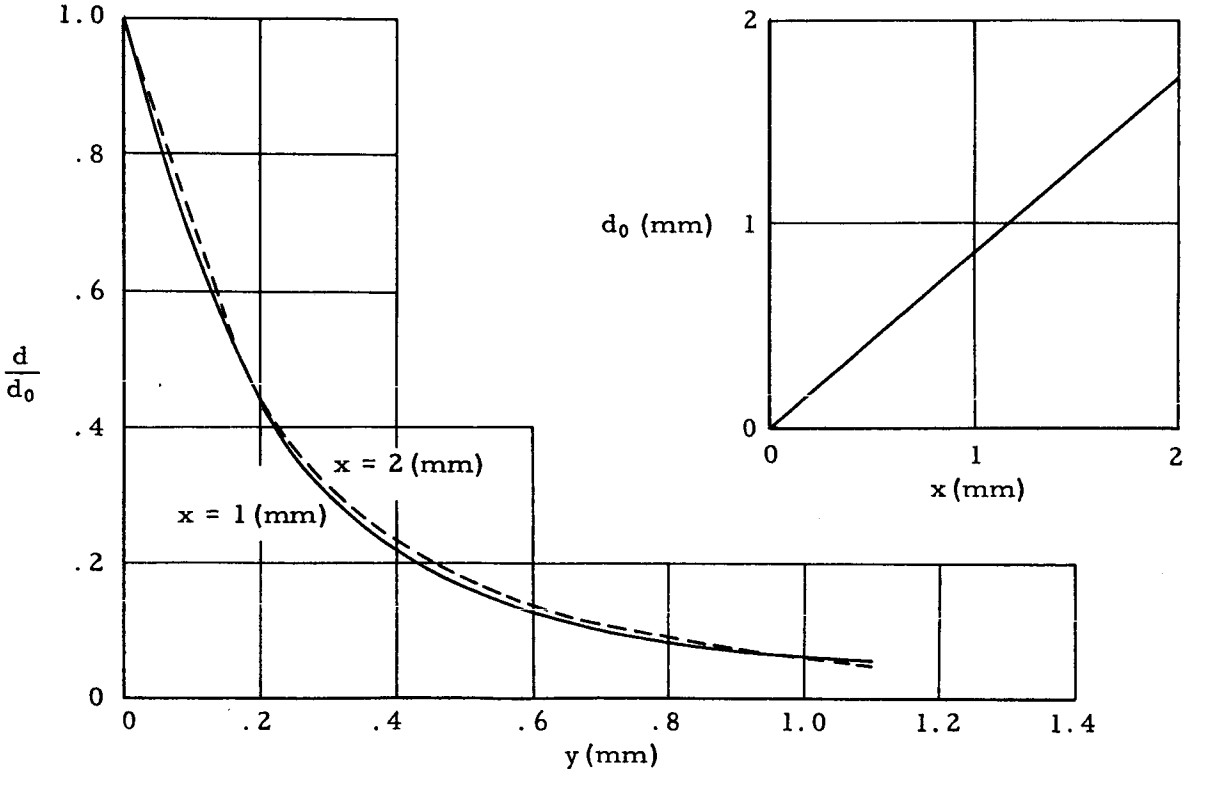

FIG. 21. STRIAE DEFORMATION FOR PARTICULAR TEKTITE TRAJECTORY, (54% MASS LOSS)

Data pertains to initially hemispheric model with radius R(0) = 1.30 cm, i.e. W(0) = 11.04 grams, entry speed V_i = 6 km/sec, entry angle θ_i = 2°, and vapor pressure $p_{v1}(T)$.

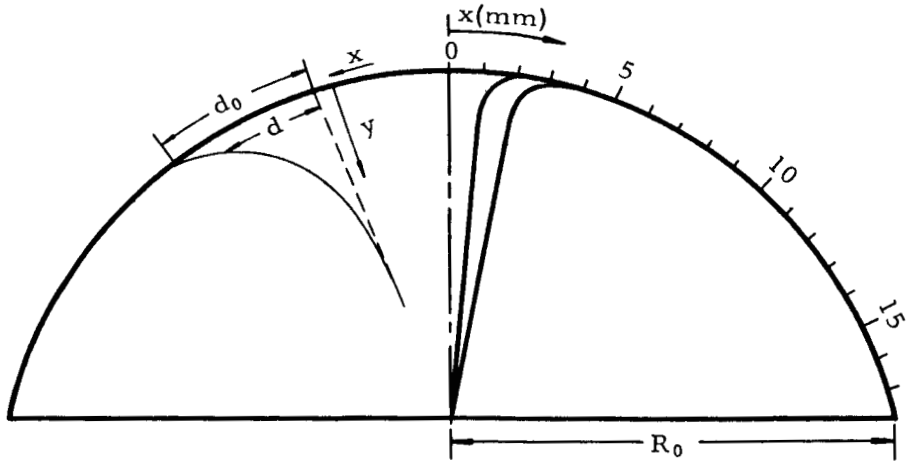

Fig. 22a. Striae After Solidification of Melt

Fig. 22c. Striae Distortion as a Function of y

Fig. 22b. Striae Distortion at the Surface as a Function of x

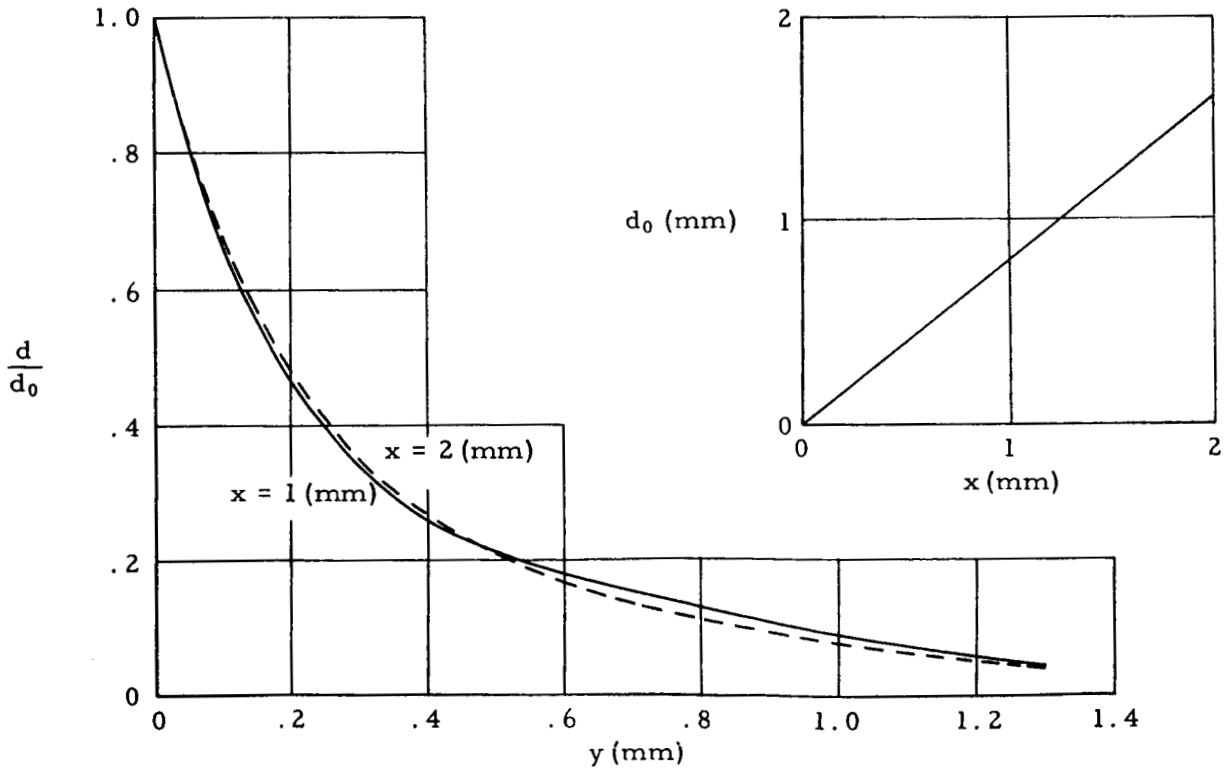

FIG. 22. STRIAE DEFORMATION FOR PARTICULAR TEKTITE TRAJECTORY, (28% MASS LOSS)

Temperature profiles pertain to time t = 35 sec, i.e. altitude H = 85.31 km of descending phase of parent meteor's skipping flight. The temperature T_s = 2033 °K of the boiling surface is determined by the equality $p_e = p_v$. Presented functions: temperature profile for α = 100 (———), temperature profile for α = 1000 (– – – –), and temperature profile for $\alpha = \infty$ (——·——), where α is the absorption coefficient for thermal radiation per meter.

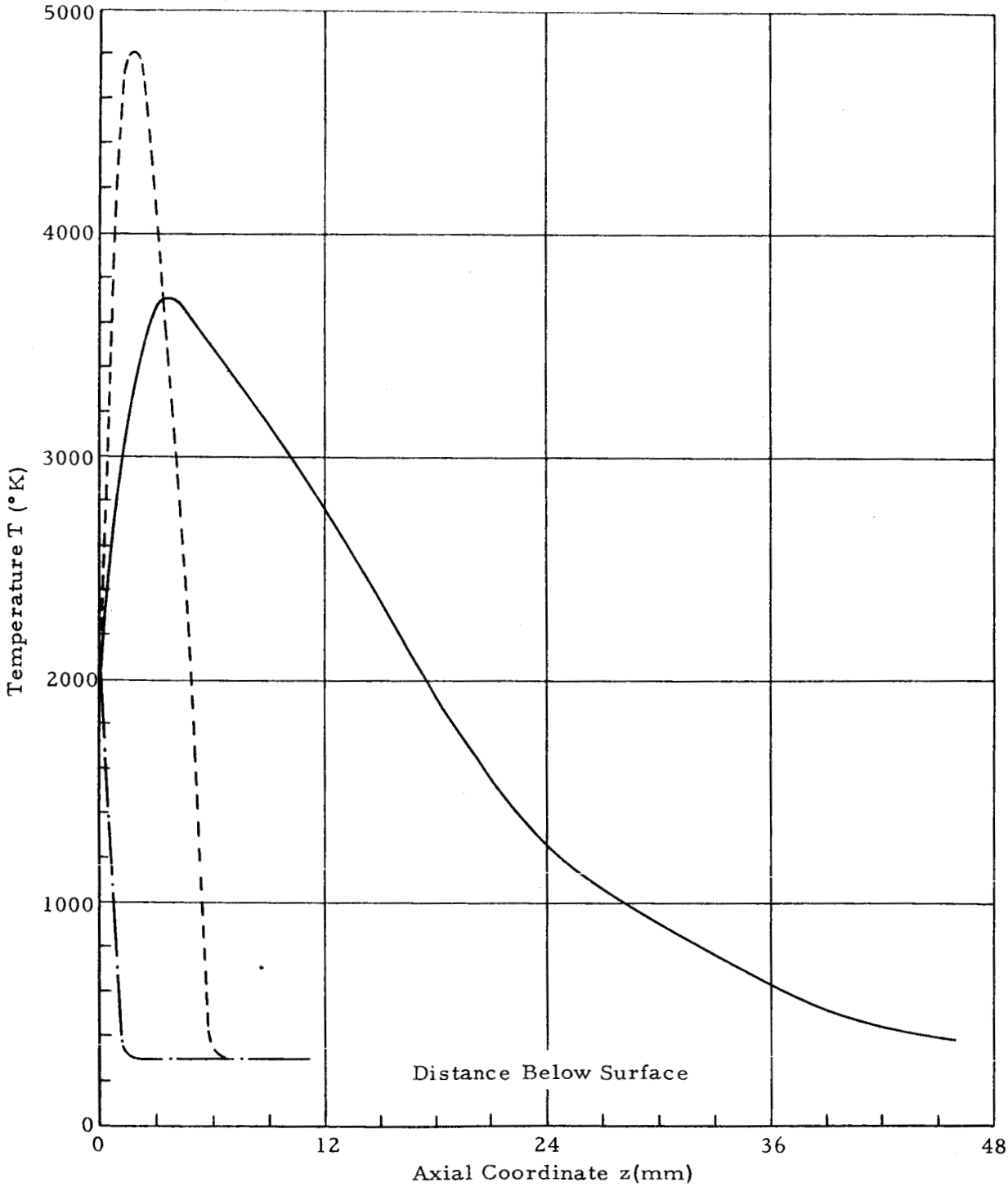

FIG. 23. TEMPERATURE DISTRIBUTION ALONG AXIS OF PARENT METEOR